JKO for Landau: a variational particle method for homogeneous Landau equation [*]

Yan Huang [†]and Li Wang [‡]

Abstract

Inspired by the gradient flow viewpoint of the Landau equation and corresponding dynamic formulation of the Landau metric in [7], we develop a novel implicit particle method for the Landau equation in the framework of the JKO scheme. We first reformulate the Landau metric in a computationally friendly form, and then translate it into the Lagrangian viewpoint using the flow map. A key observation is that, while the flow map evolves according to a rather complicated integral equation, the unknown component is merely a score function of the corresponding density plus an additional term in the null space of the collision kernel. This insight guides us in approximating the flow map with a neural network and simplifies the training. Additionally, the objective function is in a double summation form, making it highly suitable for stochastic methods. Consequently, we design a tailored version of stochastic gradient descent that maintains particle interactions and reduces the computational complexity. Compared to other deterministic particle methods, the proposed method enjoys exact entropy dissipation and unconditional stability, therefore making it suitable for large-scale plasma simulations over extended time periods.

Key words. particle method, Landau equation, gradient flows, neural network, stochastic optimization

MSC codes. 65M75, 82C40, 82D10, 82M30, 68T07

1 Introduction

The Landau equation is a fundamental kinetic equation used to model the behavior of charged particles interacting via Coulomb forces [28]. It is especially relevant for plasmas where collision effects can be significant. When spatial dependence is ignored, the Landau equation takes the following form:

$$\partial_t f = \underbrace{\nabla_{\boldsymbol{v}} \cdot \left[\int_{\mathbb{R}^d} A(\boldsymbol{v}-\boldsymbol{v}_*) \left(f(t,\boldsymbol{v}_*) \nabla_{\boldsymbol{v}} f(t,\boldsymbol{v}) - f(t,\boldsymbol{v}) \nabla_{\boldsymbol{v}_*} f(t,\boldsymbol{v}_*) \right) \mathrm{d}\boldsymbol{v}_* \right]}_{=:Q(f,f)}, \tag{1}$$

where $f(t,\boldsymbol{v})$ for $(t,\boldsymbol{v}) \in \mathbb{R}^+ \times \mathbb{R}^d$ with $d \geq 2$, is the mass distribution function of charged particles, such as electrons or ions, at time t with velocity $\boldsymbol{v}$. The operator $Q(f,f)$ is known as the Landau collision operator, which can be derived from the Boltzmann collision operator when the small angular deviation is dominated. The collision kernel A is given by:

$$A(\boldsymbol{z}) = C_\gamma |\boldsymbol{z}|^{\gamma+2} \left(I_d - \frac{\boldsymbol{z} \otimes \boldsymbol{z}}{|\boldsymbol{z}|^2} \right) =: C_\gamma |\boldsymbol{z}|^{\gamma+2} \Pi(\boldsymbol{z}),$$

where $C_\gamma > 0$ is the collision strength, and I_d is the identity matrix. As written, $\Pi(\boldsymbol{z})$ denotes the projection into $\{\boldsymbol{z}\}^\perp$. The parameter γ ranges from $-d-1$ to 1. Specifically, $0 < \gamma \leq 1$ is associated with hard potentials, while $\gamma < 0$ corresponds to the soft potentials. Of particular interest is the case when $d = 3$ and $\gamma = -3$, which corresponds to the Coulomb interaction in plasma [14, 33]. Alternatively, $\gamma = 0$ is known as the Maxwellian case, where the equation simplifies to a degenerate linear Fokker-Planck equation [34].

The theoretical understanding of (1) remains limited and continues to be an active area of research. The well-established case is for hard potentials or Maxwellian, with seminal works [16, 17, 34] and related literature addressing both the well-posedness and regularity of the solution. Significant progress on soft potentials was made in [22], which covers the global existence and uniqueness of solutions, but only for those near the Maxwellian distribution. A recent breakthrough in [21] tackles the Coulomb case, showing that the Fisher

[*]This work is partially supported by NSF grant DMS-1846854 and UMN DSI-SSG-4886888864.

[†]School of Mathematics, University of Minnesota Twin Cities, Minneapolis, MN 55455, USA. (huan2728@umn.edu)

[‡]School of Mathematics, University of Minnesota Twin Cities, Minneapolis, MN 55455, USA. (liwang@umn.edu)

information is monotonically decreasing over time, thereby ensuring that the solution remains globally bounded in time.

The numerical computation of (1) also presents significant challenges due to the complexity of the operator Q, the high dimensionality in $\boldsymbol{v}$, and the need to preserve the physical properties of the solution. Previous efforts have included methods such as the Fourier-Galerkin spectral method [32], the direct simulation Monte Carlo method [18], the finite difference entropy method [15, 5], and the deterministic particle methods [8], each addressing various aspects of these challenges.

In this paper, we aim to develop a method that simultaneously addresses all these challenges. Our approach builds upon the novel gradient flow perspective of (1) introduced in [7], ensuring that it is structure-preserving by design. To handle high dimensions more efficiently, our method is particle-based and incorporates the approximation capabilities of neural networks. Unlike many physics-based machine learning approaches for solving PDEs, our use of neural networks is minimal, therefore significantly simplifying the training process. Comparing to recent efforts that also employ neural networks for solving the Landau equation [24, 25], our method differs primarily in its design of an implicit scheme rather than an explicit one. As a result, our method is unconditionally stable and exact entropy-dissipative, making it highly suitable for large-scale time simulations of plasma.

To lay out the main idea of our method, we briefly revisit the derivation of the Landau equation as a gradient flow [7], in a formal language. First rewrite Q in the log form

$$Q(f,f) = \nabla\cdot\left[\int_{\mathbb{R}^d} A(\boldsymbol{v}-\boldsymbol{v}_*)(\nabla\log f - \nabla_*\log f_*)ff_*\mathrm{d}\boldsymbol{v}_*\right],$$

where the following abbreviated notations are used:

$$f := f(t,\boldsymbol{v}),\ f_* := f(t,\boldsymbol{v}_*),\ \nabla := \nabla_{\boldsymbol{v}},\ \nabla_* := \nabla_{\boldsymbol{v}_*}.$$

For an appropriate test function $\varphi=\varphi(\boldsymbol{v})$, (1) admits the following weak form:

$$\frac{\mathrm{d}}{\mathrm{d}t}\int_{\mathbb{R}^d}\varphi f\mathrm{d}\boldsymbol{v} = -\frac{1}{2}\iint_{\mathbb{R}^{2d}}(\nabla\varphi-\nabla_*\varphi_*)\cdot A(\boldsymbol{v}-\boldsymbol{v}_*)(\nabla\log f-\nabla_*\log f_*)ff_*\mathrm{d}\boldsymbol{v}\mathrm{d}\boldsymbol{v}_*\,. \tag{2}$$

Choosing $\varphi(\boldsymbol{v}) = 1, \boldsymbol{v}, |\boldsymbol{v}|^2$ leads to the conservation of mass, momentum and energy. Inserting $\varphi(\boldsymbol{v}) = \log f(\boldsymbol{v})$, one obtains the entropy decay due to the fact that A is symmetric and semi-positive definite.

Define a new gradient operator:

$$\tilde{\nabla}\varphi := \sqrt{C_\gamma}|\boldsymbol{v}-\boldsymbol{v}_*|^{1+\gamma/2}\Pi(\boldsymbol{v}-\boldsymbol{v}_*)(\nabla\varphi-\nabla_*\varphi_*)\,. \tag{3}$$

Since $\Pi^2=\Pi$, the weak form (2) can be rewritten into

$$\frac{\mathrm{d}}{\mathrm{d}t}\int_{\mathbb{R}^d}\varphi f\mathrm{d}\boldsymbol{v} = -\frac{1}{2}\iint_{\mathbb{R}^{2d}}\tilde{\nabla}\varphi\cdot\tilde{\nabla}\frac{\delta\mathcal{H}}{\delta f}ff_*\mathrm{d}\boldsymbol{v}\mathrm{d}\boldsymbol{v}_*\,,\ \mathcal{H}=\int_{\mathbb{R}^d}f\log f\mathrm{d}\boldsymbol{v}\,, \tag{4}$$

where $\tilde{\nabla}\cdot$ is the corresponding divergence operator in the distributional sense. More specifically, given a test function $\varphi(\boldsymbol{v})\in C_c^\infty(\mathbb{R}^d)$ and a vector-valued function $\psi=\psi(\boldsymbol{v},\boldsymbol{v}_*)\in\mathbb{R}^d$, we have:

$$\iint_{\mathbb{R}^{2d}}\tilde{\nabla}\varphi(\boldsymbol{v},\boldsymbol{v}_*)\cdot\psi(\boldsymbol{v},\boldsymbol{v}_*)\mathrm{d}\boldsymbol{v}_*\mathrm{d}\boldsymbol{v} = -\int_{\mathbb{R}^d}\varphi(\boldsymbol{v})(\tilde{\nabla}\cdot\psi)(\boldsymbol{v})\mathrm{d}\boldsymbol{v}\,. \tag{5}$$

Equipped with this notation, one can rewrite the Landau equation (1) as

$$\partial_t f + \frac{1}{2}\tilde{\nabla}\cdot\left(ff_*\tilde{\nabla}\frac{\delta\mathcal{H}}{\delta f}\right) = 0\,. \tag{6}$$

Now drawing an analogy to the Wasserstein gradient flow perspective on the heat equation, [7] defines the following Landau metric between two probability densities f_0 and f_1 [1], denoted as d_L:

$$\begin{aligned} d_L^2(f_0,f_1) :=& \inf_{f,V}\left\{\frac{1}{2}\int_0^1\iint_{\mathbb{R}^{2d}}|V|^2ff_*\mathrm{d}\boldsymbol{v}\mathrm{d}\boldsymbol{v}_*\mathrm{d}t\right\}, \\ & s.t.\ \ \partial_t f + \frac{1}{2}\tilde{\nabla}\cdot(Vff_*) = 0\,,\ f(0,\cdot)=f_0\,,\ f(1,\cdot)=f_1\,. \end{aligned} \tag{7}$$

As a result, the Landau equation (1) can be viewed as the gradient flow of entropy $\mathcal{H}$ with respect to the metric d_L. In particular, one can construct the weak solution of (1) by De Giorgi's minimizing movement scheme [1],

[1] In this paper, we do not distinguish between the notation for probability measures and densities.

commonly known as the Jordan-Kinderlehrer-Otto (JKO) scheme [27]. Specifically, fix a time step $\tau > 0$, one recursively defines a sequence $\{f^n\}_{n=0}^{\infty}$ as

$$f^0 = f(0,\cdot)\,,\ f^{n+1} \in \arg\inf_{f} \left[d_L^2(f, f^n) + 2\tau\mathcal{H}(f)\right]\,. \tag{8}$$

The resulting solution will be a time-discrete approximation of (1), and with appropriate time interpolation, it will converge to the solution of (1) as $\tau \to 0$ under certain conditions. More rigorous statements will be given in Section 2.1.

Our numerical scheme is based on the formulations in (8) and (7). However, although (7) resembles the Benamou–Brenier's dynamic formulation of the 2-Wasserstein metric [3], it is not easily accessible from a computational standpoint. Therefore, we introduce the following alternative formulation of d_L:

$$\begin{aligned} d_L^2(f_0, f_1) := \inf_{f,\boldsymbol{u}} \frac{1}{2}\int_0^1 \iint_{\mathbb{R}^{2d}} |\boldsymbol{u}-\boldsymbol{u}_*|_A^2 f f_* \mathrm{d}\boldsymbol{v}\mathrm{d}\boldsymbol{v}_*\mathrm{d}t\,, \\ s.t.\ \ \partial_t f = \nabla\cdot\left[f\left(\int_{\mathbb{R}^d} A(\boldsymbol{v}-\boldsymbol{v}_*)(\boldsymbol{u}-\boldsymbol{u}_*)f_*\mathrm{d}\boldsymbol{v}_*\right)\right]\,,\ f(0,\cdot)=f_0\,,\ f(1,\cdot)=f_1\,, \end{aligned} \tag{9}$$

such that the complex expression of $\tilde{\nabla}$ is explicitly spelled out. A more detailed relation between (7) and (9) will be outlined in Section 2.1.

A key advantage of the new form (9) is that both the objective function and the constrained PDE can be represented using particles. This is significant because particle methods, unlike grid-based methods, tend to scale better with dimensionality. Specifically, the objective function, which involves a double integral, can be interpreted as a double expectation with respect to the probability densities f and f_*. This allows it to be approximated by the empirical sum of particles. Similarly, the constrained PDE can be viewed as a transport equation with an integral form of the velocity field, which can also be interpreted as an expectation and thus approximated using particles.

To update the particle velocities sequentially in time, we use the flow map representation, as previously adopted in [29]. This approach has two favorable traits: First, it propagates both the particles and the density simultaneously, completely avoiding the challenges associated with density estimation, which is often a bottleneck in particle-based methods. Second, it transforms the constrained optimization problem (9) into an unconstrained one, allowing optimization with respect to the flow map (or more specifically $\boldsymbol{u}$ that generates the flow map) instead of both f and $\boldsymbol{u}$. This broadens the range of available optimization solvers and simplifies the optimization process.

In practice, $\boldsymbol{u}$ is approximated by a neural network, which offers greater flexibility and is less sensitive to dimensionality compared to other approximations such as polynomials or Fourier series. Additionally, due to the particle representation in (9), the training process is well-suited to stochastic methods. Specifically, we design a tailored mini-batch stochastic gradient descent (SGD), inspired by the standard mini-batch SGD [4]. We also provide corresponding convergence analysis under common optimization theory assumptions. Once $\boldsymbol{u}$ is trained, the particle update can be performed with improved efficiency using the random batch method [26].

The rest of the paper is organized as follows. In the next section, we present key components in the design of our method. We begin with a review of the gradient flow perspective of the Landau equation and the dynamic formulation of the Landau metric. We then convert the Landau metric into a computable form and reformulate it using Lagrangian coordinates. This new metric, combined with the JKO scheme, forms the foundation of our variational approach. In Section 3, we detail our scheme, which includes a particle method and a neural network approximation. Since the objective function for training the neural network is in the form of a double summation. Section 4 focuses on the stochastic optimization method and its convergence. Extensive numerical tests are presented in Section 5.

2 Variational formulation and the JKO scheme

This section outlines the foundational elements of our method. We first summarize the theoretical results from [7], which establish the basis for viewing the Landau equation as a gradient flow. We also derive a more computationally friendly version of the Landau metric. This gradient flow perspective will then be translated into a dynamical JKO scheme, where we verify that the Landau equation is recovered up to first-order accuracy in time, based on the optimality conditions. Finally, we introduce a Lagrangian formulation in preparation for spatial discretization.

2.1 Gradient flow perspective

Let $\mathcal{P}_2(\mathbb{R}^d)$ be the space of probability measures with finite 2-moments: $\mathcal{P}_2(\mathbb{R}^d) := \big\{f : f \in \mathcal{P}(\mathbb{R}^d)\,, m_2(f) := \int_{\mathbb{R}^d} |\boldsymbol{v}|^2 \mathrm{d}f < \infty\big\}$. When the second moment is bounded by E, we denote this space to be $\mathcal{P}_{2,E}(\mathbb{R}^d) \subset \mathcal{P}_2(\mathbb{R}^d)$.

Following Villani's H-solutions [33], the notion of a weak solution to (1) is defined as:

Definition 1. *[7, Definition 1] For $T > 0$, we say that $f \in C([0,T]; L^1(\mathbb{R}^d))$ is a weak solution to the Landau equation* (1) *if for every test function $\varphi \in C_c^\infty((0,T) \times \mathbb{R}^d)$, we have $\int_0^T \int_{\mathbb{R}^d} \partial_t \varphi f \mathrm{d}\boldsymbol{v} \mathrm{d}t = \frac{1}{2} \int_0^T \iint_{\mathbb{R}^{2d}} \tilde{\nabla}\varphi \cdot \tilde{\nabla} \frac{\delta \mathcal{H}}{\delta f} f f_* \mathrm{d}\boldsymbol{v} \mathrm{d}\boldsymbol{v}_* \mathrm{d}t$, and f satisfies the following properties:*

(i) f is a probability measure with uniformly bounded second moment;

(ii) The entropy $\mathcal{H}(f) := \int_{\mathbb{R}^d} f \log f \mathrm{d}\boldsymbol{v}$ is bounded: $\mathcal{H}(f(t,\cdot)) \le \mathcal{H}(f(0,\cdot)) < +\infty$ for all $t \in [0,T]$;

(iii) The entropy dissipation is time integrable:

$$D_{\mathcal{H}}(f) := \frac{1}{2} \int_0^T \iint_{\mathbb{R}^d} \left| \tilde{\nabla} \frac{\delta \mathcal{H}}{\delta f} \right|^2 f f_* \mathrm{d}\boldsymbol{v} \mathrm{d}\boldsymbol{v}_* \mathrm{d}t < \infty \,. \tag{10}$$

where operator $\tilde{\nabla}$ is defined in (3)*.*

One main theorem in [7] establishes the equivalence between the gradient flow solution (defined as the curves of maximal slope, see Definition 5) and the weak solution of the Landau equation.

Theorem 2.1 (Landau equation as a gradient flow)**.** *[7, Theorem 12] b Fix $d = 3$ and $\gamma \in (-3, 0]$. Suppose that a curve $\mu : [0,T] \to \mathcal{P}(\mathbb{R}^3)$ has a density $f(t,\boldsymbol{v})$ that satisfies the following assumptions:*

(i) For $\kappa \in (0, \gamma+3]$, we have $\langle \boldsymbol{v} \rangle^{2-\gamma} f(t,\boldsymbol{v}) \in L_t^\infty(0,T; L_{\boldsymbol{v}}^1 \cap L_{\boldsymbol{v}}^{(3-\kappa)/(3+\gamma-\kappa)}(\mathbb{R}^3))$, where $\langle \boldsymbol{v} \rangle^2 = 1 + |\boldsymbol{v}|^2$;

(ii) The initial entropy is finite: $\mathcal{H}(f(0,\cdot)) = \int_{\mathbb{R}^d} f(0,\boldsymbol{v}) \log f(0,\boldsymbol{v}) \mathrm{d}\boldsymbol{v} < \infty$;

(iii) The entropy-dissipation is time integrable, i.e, f satisfies (10)*.*

Then μ is a curve of maximal slope for $\mathcal{H}$ with respect to its strong upper gradient $\sqrt{D_{\mathcal{H}}}$ if and only if its density f is a weak solution of the homogeneous Landau equation (1)*. Moreover, we have the following energy dissipation equality:*

$$\mathcal{H}(f(t,\cdot)) + \frac{1}{2} \int_0^t |f'|_{d_L}^2(s) \mathrm{d}s + \frac{1}{2} \int_0^t D_{\mathcal{H}}(f(s,\cdot)) ds = \mathcal{H}(f(0,\cdot)) \,,$$

where $|f'|_{d_L}$ is the metric derivative of curve f with metric d_L defined in (7)*.*

For foundational theory on gradient flows, one can refer to [1, Chapter 1] and consult Appendix A for basic definitions. The key distinction here lies in the definition of the metric, which has been shown in [7, Theorem 7] to provide a meaningful topology on $\mathcal{P}_{2,E}$. As mentioned earlier, d_L in its original form is not easy to compute. Therefore, we derive an alternative form of the Landau metric.

Recall the weak form (2) of the Landau equation. If we choose $\varphi = \log f(\boldsymbol{v}) = \frac{\delta \mathcal{H}}{\delta f}$ with $\mathcal{H}$ given in (4), we get entropy decay with the decay rate $-\frac{1}{2} \iint_{\mathbb{R}^{2d}} (S - S_*) \cdot A(\boldsymbol{v} - \boldsymbol{v}_*)(S - S_*) f f_* \mathrm{d}\boldsymbol{v} \mathrm{d}\boldsymbol{v}_*$, where $S(\boldsymbol{v}) := \nabla_v \log f(\boldsymbol{v})$. This motivates the definition of an action functional

$$\frac{1}{2} \iint_{\mathbb{R}^{2d}} (\boldsymbol{u} - \boldsymbol{u}_*) \cdot A(\boldsymbol{v} - \boldsymbol{v}_*)(\boldsymbol{u} - \boldsymbol{u}_*) f f_* \mathrm{d}\boldsymbol{v} \mathrm{d}\boldsymbol{v}_* \,, \text{ where } \boldsymbol{u} = \boldsymbol{u}(\boldsymbol{v}),\ \boldsymbol{u}_* = \boldsymbol{u}(\boldsymbol{v}_*) \,. \tag{11}$$

Following the minimizing action principle, one can minimize the action (11) over the curves that satisfy an appropriate continuity equation to derive the Landau metric. To construct such continuity equation, we interpret the Landau equation as a continuity equation with an integral velocity field, i.e.,

$$\partial_t f = \nabla \cdot \left[f \left(\int_{\mathbb{R}^d} A(\boldsymbol{v} - \boldsymbol{v}_*)(\boldsymbol{u} - \boldsymbol{u}_*) f_* \mathrm{d}\boldsymbol{v}_* \right) \right] . \tag{12}$$

The combination of (11) and (12) then gives rise to the Landau metric (9).

A more direct relation between (7) and (9) is to observe that, by comparing the constrained equation in (7) with the Landau equation (6), we see that V corresponds to $\tilde{\nabla} \frac{\delta \mathcal{H}}{\delta f}$. Therefore, we can assume V admits the following form:

$$V = \tilde{\nabla}\phi = \sqrt{C_\gamma} |\boldsymbol{v} - \boldsymbol{v}_*|^{1+\gamma/2} \Pi(\boldsymbol{v} - \boldsymbol{v}_*)(\nabla\phi - \nabla_*\phi_*) \,,$$

for some function $\phi = \phi(t,\boldsymbol{v})$. This is analogous to the fact that the optimal vector field in 2-Wasserstein metric is the gradient of some potential function [35]. Denote $\boldsymbol{u} := \nabla\phi$ and $|\boldsymbol{u} - \boldsymbol{u}_*|_A^2 := (\boldsymbol{u} - \boldsymbol{u}_*) \cdot A(\boldsymbol{v} - \boldsymbol{v}_*)(\boldsymbol{u} - \boldsymbol{u}_*)$. Then (9) directly follows from (7).

2.2 Dynamical JKO scheme

With the definition of the Landau metric established, we can now formulate the dynamical JKO scheme. This approach was first explored as a viable numerical method for Wasserstein gradient flow in [6] and subsequently in [11] for more general metric.

Problem 1 (dynamical JKO scheme)**.** *Given f^n, solve $f^{n+1} := f(1,\cdot)$ by*

$$\begin{cases} \displaystyle\inf_{f,\boldsymbol{u}} \frac{1}{2}\int_0^1 \iint_{\mathbb{R}^{2d}} |\boldsymbol{u}-\boldsymbol{u}_*|_A^2 f f_* \mathrm{d}\boldsymbol{v}\mathrm{d}\boldsymbol{v}_*\mathrm{d}t + 2\tau\mathcal{H}(f(1,\cdot))\,, \\ s.t. \quad \partial_t f = \nabla\cdot\left[f\left(\displaystyle\int_{\mathbb{R}^d} A(\boldsymbol{v}-\boldsymbol{v}_*)(\boldsymbol{u}-\boldsymbol{u}_*)f_*\mathrm{d}\boldsymbol{v}_*\right)\right]\,,\ f(0,\cdot)=f^n\,. \end{cases} \tag{13}$$

As with the vanilla JKO scheme, the (13) enjoys structure-preserving property.

Proposition 2.2. *Formulation* (13) *has the following properties for any $n \geq 0$:*

(i) Entropy dissipation: $\mathcal{H}(f^{n+1}) \leq \mathcal{H}(f^n)$.

(ii) Mass, momentum, and energy conservation:

$$\int_{\mathbb{R}^d} \varphi(\boldsymbol{v}) f^{n+1}(\boldsymbol{v})\mathrm{d}\boldsymbol{v} = \int_{\mathbb{R}^d} \varphi(\boldsymbol{v}) f^n(\boldsymbol{v})\mathrm{d}\boldsymbol{v},\ \textit{for } \varphi(\boldsymbol{v}) = 1\,,\boldsymbol{v}\,,|\boldsymbol{v}|^2\,.$$

Proof. Property (i) is a direct consequence of the fact that f^{n+1} is a minimizer. Property (ii) is guaranteed by the constraint PDE: for $\varphi(\boldsymbol{v}) = 1\,,\boldsymbol{v}\,,|\boldsymbol{v}|^2$,

$$\begin{aligned} \frac{\mathrm{d}}{\mathrm{d}t}\int_{\mathbb{R}^d} f\varphi\mathrm{d}\boldsymbol{v} &= \int_{\mathbb{R}^d} \varphi\nabla\cdot\left[f\left(\int_{\mathbb{R}^d} A(\boldsymbol{v}-\boldsymbol{v}_*)(\boldsymbol{u}-\boldsymbol{u}_*)f_*\mathrm{d}\boldsymbol{v}_*\right)\right]\mathrm{d}\boldsymbol{v} \\ &= -\iint_{\mathbb{R}^{2d}} \nabla\varphi\cdot A(\boldsymbol{v}-\boldsymbol{v}_*)(\boldsymbol{u}-\boldsymbol{u}_*)ff_*\mathrm{d}\boldsymbol{v}\mathrm{d}\boldsymbol{v}_* \\ &= -\frac{1}{2}\iint_{\mathbb{R}^{2d}} (\nabla\varphi-\nabla_*\varphi_*)\cdot A(\boldsymbol{v}-\boldsymbol{v}_*)(\boldsymbol{u}-\boldsymbol{u}_*)ff_*\mathrm{d}\boldsymbol{v}\mathrm{d}\boldsymbol{v}_* = 0\,. \end{aligned}$$

□

We now demonstrate that (13) indeed provides a first-order in τ approximation to (1). Let $\lambda(t,\boldsymbol{v})$ be the Lagrangian multiplier, the Lagrangian associated with (13) is given by:

$$\begin{aligned} \mathcal{L}(f,\boldsymbol{u},\lambda) &= \frac{1}{2}\int_0^1\iint_{\mathbb{R}^{2d}} (\boldsymbol{u}-\boldsymbol{u}_*)\cdot A(\boldsymbol{v}-\boldsymbol{v}_*)(\boldsymbol{u}-\boldsymbol{u}_*)ff_*\mathrm{d}\boldsymbol{v}\mathrm{d}\boldsymbol{v}_*\mathrm{d}t + 2\tau\mathcal{H}(f(1,\cdot)) \\ &\quad + \int_0^1\int_{\mathbb{R}^d} \lambda\left[\partial_t f - \nabla\cdot\left(f\int_{\mathbb{R}^d} A(\boldsymbol{v}-\boldsymbol{v}_*)(\boldsymbol{u}-\boldsymbol{u}_*)f_*\mathrm{d}\boldsymbol{v}_*\right)\right]\mathrm{d}\boldsymbol{v}\mathrm{d}t \\ &= \frac{1}{2}\int_0^1\iint_{\mathbb{R}^{2d}} (\boldsymbol{u}-\boldsymbol{u}_*+\nabla\lambda-\nabla_*\lambda_*)\cdot A(\boldsymbol{v}-\boldsymbol{v}_*)(\boldsymbol{u}-\boldsymbol{u}_*)ff_*\mathrm{d}\boldsymbol{v}\mathrm{d}\boldsymbol{v}_*\mathrm{d}t \\ &\quad - \int_0^1\int_{\mathbb{R}^d} f\partial_t\lambda\mathrm{d}\boldsymbol{v}\mathrm{d}t + \int_{\mathbb{R}^d} f\lambda|_{t=0}^{t=1}\mathrm{d}\boldsymbol{v} + 2\tau\mathcal{H}(f(1,\cdot))\,. \end{aligned}$$

By definition, the variation of $\mathcal{L}$ with respect to $\boldsymbol{u}$ is calculated via

$$\begin{aligned} \int_0^1\int_{\mathbb{R}^d} \eta\frac{\delta\mathcal{L}}{\delta\boldsymbol{u}}\mathrm{d}\boldsymbol{v}\mathrm{d}t &= \lim_{\varepsilon\to 0}\frac{\mathcal{L}(f,\boldsymbol{u}+\varepsilon\eta,\lambda)-\mathcal{L}(f,\boldsymbol{u},\lambda)}{\varepsilon} \\ &= \frac{1}{2}\int_0^1\iint_{\mathbb{R}^{2d}} (2\boldsymbol{u}-2\boldsymbol{u}_*+\nabla\lambda-\nabla_*\lambda_*)\cdot A(\boldsymbol{v}-\boldsymbol{v}_*)(\eta-\eta_*)ff_*\mathrm{d}\boldsymbol{v}\mathrm{d}\boldsymbol{v}_*\mathrm{d}t \\ &= \int_0^1\int_{\mathbb{R}^d} \eta\left[f\left(\int_{\mathbb{R}^d} A(\boldsymbol{v}-\boldsymbol{v}_*)(2\boldsymbol{u}-2\boldsymbol{u}_*+\nabla\lambda-\nabla_*\lambda_*)f_*\mathrm{d}\boldsymbol{v}_*\right)\right]\mathrm{d}\boldsymbol{v}\mathrm{d}t\,. \end{aligned}$$

Therefore, the first-order optimality condition writes as:

$$\frac{\delta\mathcal{L}}{\delta\boldsymbol{u}} = f\left(\int_{\mathbb{R}^d} A(\boldsymbol{v}-\boldsymbol{v}_*)(2\boldsymbol{u}-2\boldsymbol{u}_*+\nabla\lambda-\nabla_*\lambda_*)f_*\mathrm{d}\boldsymbol{v}_*\right) = 0\,. \tag{14}$$

Likewise, we have the other two optimality conditions:

$$\frac{\delta \mathcal{L}}{\delta f} = -\partial_t \lambda + \int_{\mathbb{R}^d} (\boldsymbol{u} - \boldsymbol{u}_* + \nabla\lambda - \nabla_*\lambda_*) \cdot A(\boldsymbol{v} - \boldsymbol{v}_*)(\boldsymbol{u} - \boldsymbol{u}_*) f_* \mathrm{d}\boldsymbol{v}_* = 0\,, \tag{15}$$

$$\frac{\delta \mathcal{L}}{\delta f(1,\cdot)} = \lambda(1,\cdot) + 2\tau \frac{\delta \mathcal{H}(f(1,\cdot))}{\delta f(1,\cdot)} = \lambda(1,\cdot) + 2\tau \log f(1,\cdot) = 0\,. \tag{16}$$

Lemma 2.3. *If $\varphi(\boldsymbol{v}) : \mathbb{R}^d \to \mathbb{R}^d$ satisfies $\int_{\mathbb{R}^d} A(\boldsymbol{v} - \boldsymbol{v}_*)(\varphi - \varphi_*) f_* \mathrm{d}\boldsymbol{v}_* = 0$, then $\varphi \in span\{\mathbf{1}, \boldsymbol{v}\}$ on the support of f.*

Proof. Integrating this equality against $f\mathrm{d}\boldsymbol{v}$, we have

$$0 = \iint_{\mathbb{R}^{2d}} \varphi \cdot A(\boldsymbol{v} - \boldsymbol{v}_*)(\varphi - \varphi_*) f_* f \mathrm{d}\boldsymbol{v}_* \mathrm{d}\boldsymbol{v} = \frac{1}{2} \iint_{\mathbb{R}^{2d}} (\varphi - \varphi_*) \cdot A(\boldsymbol{v} - \boldsymbol{v}_*)(\varphi - \varphi_*) f_* f \mathrm{d}\boldsymbol{v}_* \mathrm{d}\boldsymbol{v}\,.$$

Since A is semi-positive definite, this implies $A(\boldsymbol{v} - \boldsymbol{v}_*)(\varphi - \varphi_*) = 0$ on the support of $f_* f$. Therefore, $\varphi \in span\{\mathbf{1}, \boldsymbol{v}\}$ on the support of f. □

By Lemma 2.3, (14) implies that $2\boldsymbol{u} + \nabla\lambda \in span\{\mathbf{1}, \boldsymbol{v}\}$ on *supp* (f). Combined with (16), this shows that

$$\boldsymbol{u}(1, \boldsymbol{v}) \in \tau \nabla \log f(1, \boldsymbol{v}) + span\{\mathbf{1}, \boldsymbol{v}\} \quad \text{on} \quad supp\ (f)\,. \tag{17}$$

Substituting (17) into the constraint PDE in (13) reveals that $f^{n+1} = f(1,\cdot)$ is indeed the solution of the homogeneous Landau equation (1) after one time step τ. Additionally, (15) shows that λ satisfies following equation

$$\partial_t \lambda + \frac{1}{4} \int_{\mathbb{R}^d} |\nabla\lambda - \nabla_*\lambda_*|_A^2 f_* \mathrm{d}\boldsymbol{v}_* = 0\,.$$

This can be viewed as a generalization of the Hamilton-Jacobi equation that the dual variable must satisfy in the 2-Wasserstein metric.

2.3 Lagrangian formulation

To facilitate the particle method in the next section, we translate the variational problem (13) into the corresponding Lagrange formulation, following [10, 29]. Assume the velocity field is sufficiently regular, then the solution $f(t, \boldsymbol{v})$ to the constrained continuity equation can be represented as

$$f(t,\cdot) = T_{t\#} f^n\,,\ t \in [0,1]\,,$$

where T_t is the flow map that solves the following ODE:

$$\frac{\mathrm{d}}{\mathrm{d}t} T_t(\boldsymbol{v}) = -\int_{\mathbb{R}^d} A(T_t(\boldsymbol{v}) - T_t(\boldsymbol{v}_*))[\boldsymbol{u}(t, T_t(\boldsymbol{v})) - \boldsymbol{u}(t, T_t(\boldsymbol{v}_*))] f_*^n \mathrm{d}\boldsymbol{v}_*\,, \tag{18}$$

with $T_0(\boldsymbol{v}) = \boldsymbol{v}$. The entropy term in (13) can also be represented using map T_t:

$$\begin{aligned}
\mathcal{H}(T_{1\#} f^n) = \mathcal{H}(f(1,\cdot)) &= \int_{\mathbb{R}^d} f(1, \boldsymbol{v}) \log f(1, \boldsymbol{v}) \mathrm{d}\boldsymbol{v} \\
&= \int_{\mathbb{R}^d} [f(1, T_1(\boldsymbol{v})) \log f(1, T_1(\boldsymbol{v}))] |\det \nabla_{\boldsymbol{v}} T_1(\boldsymbol{v})| \mathrm{d}\boldsymbol{v} \\
&= \int_{\mathbb{R}^d} \log\left(\frac{f^n(\boldsymbol{v})}{|\det \nabla_{\boldsymbol{v}} T_1(\boldsymbol{v})|}\right) f^n(\boldsymbol{v}) \mathrm{d}\boldsymbol{v} \\
&= \int_{\mathbb{R}^d} f^n(\boldsymbol{v}) \log f^n(\boldsymbol{v}) \mathrm{d}\boldsymbol{v} - \int_{\mathbb{R}^d} f^n(\boldsymbol{v}) \log |\det \nabla_{\boldsymbol{v}} T_1(\boldsymbol{v})| \mathrm{d}\boldsymbol{v}\,,
\end{aligned}$$

where we have used the change of variable formula $f(1, T_1(\boldsymbol{v}))|\det \nabla_{\boldsymbol{v}} T_1(\boldsymbol{v})| = f^n(\boldsymbol{v})$. In practice, $\int_{\mathbb{R}^d} f^n(\boldsymbol{v}) \log f^n(\boldsymbol{v}) \mathrm{d}\boldsymbol{v}$ is dropped in optimization since it is independent of $\boldsymbol{u}$. To efficiently compute $|\det \nabla_{\boldsymbol{v}} T_1(\boldsymbol{v})|$, we cite a formula in [24] on the evolution of the log determinant, inspired by the concept of continuous normalizing flow [13, 20, 29].

Proposition 2.4. *[24, Corollary 4.2] Assume the map $T(t,\cdot)$ in (18) is invertible, then the log determinant of its gradient satisfies the following equation:*

$$\begin{aligned}
\frac{\mathrm{d}}{\mathrm{d}t} |\log\det \nabla_{\boldsymbol{v}} T_t(\boldsymbol{v})| = -\int_{\mathbb{R}^d} \Big\{ & A(T_t(\boldsymbol{v}) - T_t(\boldsymbol{v}_*)) : \nabla \boldsymbol{u}(t, T_t(\boldsymbol{v})) - (d-1) C_\gamma \\
& |T_t(\boldsymbol{v}) - T_t(\boldsymbol{v}_*)|^\gamma (T_t(\boldsymbol{v}) - T_t(\boldsymbol{v}_*)) \cdot [\boldsymbol{u}(t, T_t(\boldsymbol{v})) - \boldsymbol{u}(t, T_t(\boldsymbol{v}_*))] \Big\} f_*^n \mathrm{d}\boldsymbol{v}_*\,,
\end{aligned}$$

where $A : B := \sum_{ij} A_{ij} B_{ij}$.

As a result, we propose the following Lagrangian JKO scheme.

Problem 2 (dynamical JKO scheme in Lagrangian formulation)**.** *Given f^n, find the optimal T_t^{n+1} by solving*

$$\begin{cases} \inf_{\boldsymbol{u}} \ \frac{1}{2}\int_0^1 \iint_{\mathbb{R}^{2d}} |\boldsymbol{u}(t,T_t(\boldsymbol{v}))-\boldsymbol{u}(t,T_t(\boldsymbol{v}_*))|_A^2 f^n f_*^n \mathrm{d}\boldsymbol{v}\mathrm{d}\boldsymbol{v}_*\mathrm{d}t - 2\tau\int_{\mathbb{R}^d} f^n \log|\det\nabla_{\boldsymbol{v}}T_1(\boldsymbol{v})|\mathrm{d}\boldsymbol{v}\,, \\ s.t. \ \ \frac{\mathrm{d}}{\mathrm{d}t}T_t(\boldsymbol{v}) = -\int_{\mathbb{R}^d} A(T_t(\boldsymbol{v})-T_t(\boldsymbol{v}_*))[\boldsymbol{u}(t,T_t(\boldsymbol{v}))-\boldsymbol{u}(t,T_t(\boldsymbol{v}_*))]f_*^n\mathrm{d}\boldsymbol{v}_*\,, \\ \frac{\mathrm{d}}{\mathrm{d}t}\log|\det\nabla_{\boldsymbol{v}}T_t(\boldsymbol{v})| = -\int_{\mathbb{R}^d}\Big\{A(T_t(\boldsymbol{v})-T_t(\boldsymbol{v}_*)):\nabla\boldsymbol{u}(t,T_t(\boldsymbol{v}))-(d-1)C_\gamma \\ \qquad |T_t(\boldsymbol{v})-T_t(\boldsymbol{v}_*)|^\gamma(T_t(\boldsymbol{v})-T_t(\boldsymbol{v}_*))\cdot[\boldsymbol{u}(t,T_t(\boldsymbol{v}))-\boldsymbol{u}(t,T_t(\boldsymbol{v}_*))]\Big\}f_*^n\mathrm{d}\boldsymbol{v}_*\,, \\ T_0(\boldsymbol{v})=\boldsymbol{v}\,,\ \log|\det\nabla_{\boldsymbol{v}}T_0(\boldsymbol{v})|=0\,. \end{cases} \tag{19}$$

Then $f^{n+1} := T_1^{n+1}{}_\# f^n$.

3 A particle method

In this section, we derive a fully implementable version of (19) by first discretizing $\boldsymbol{v}$ using particles, applying one-step inner time discretization, and approximating to-be-optimized $\boldsymbol{u}$ with neural networks.

3.1 Particle representation

By interpreting the integrals against $f^n\mathrm{d}\boldsymbol{v}$ and $f_*^n\mathrm{d}\boldsymbol{v}_*$ as expectations, (19) reveals a particle representation. More precisely, let $\{\boldsymbol{v}_i^n\}_{i=1}^N$ be the velocity of N particles sampled from f^n, we discretize (19) as follows.

Problem 3 (dynamical JKO scheme in particle formulation)**.** *Given $\{\boldsymbol{v}_i^n\}_{i=1}^N$ and $\{f^n(\boldsymbol{v}_i^n)\}_{i=1}^N$, find the optimal T_t^{n+1} by solving*

$$\begin{cases} \inf_{\boldsymbol{u}} \ \frac{1}{2N^2}\sum_{i=1}^N\sum_{j=1}^N\int_0^1 |\boldsymbol{u}(t,T_t(\boldsymbol{v}_i^n))-\boldsymbol{u}(t,T_t(\boldsymbol{v}_j^n))|_A^2\mathrm{d}t - \frac{2\tau}{N}\sum_{i=1}^N\log|\det\nabla_{\boldsymbol{v}}T_1(\boldsymbol{v}_i^n)|\,, \\ s.t. \ \ \frac{\mathrm{d}}{\mathrm{d}t}T_t(\boldsymbol{v}_i^n) = -\frac{1}{N}\sum_{j=1}^N A(T_t(\boldsymbol{v}_i^n)-T_t(\boldsymbol{v}_j^n))[\boldsymbol{u}(t,T_t(\boldsymbol{v}_i^n))-\boldsymbol{u}(t,T_t(\boldsymbol{v}_j^n))]\,, \\ \frac{\mathrm{d}}{\mathrm{d}t}\log|\det\nabla_{\boldsymbol{v}}T_t(\boldsymbol{v}_i^n)| = -\frac{1}{N}\sum_{j=1}^N\Big\{A(T_t(\boldsymbol{v}_i^n)-T_t(\boldsymbol{v}_j^n)):\nabla\boldsymbol{u}(t,T_t(\boldsymbol{v}_i^n))-(d-1)C_\gamma \\ \qquad |T_t(\boldsymbol{v}_i^n)-T_t(\boldsymbol{v}_j^n)|^\gamma(T_t(\boldsymbol{v}_i^n)-T_t(\boldsymbol{v}_j^n))\cdot[\boldsymbol{u}(t,T_t(\boldsymbol{v}_i^n))-\boldsymbol{u}(t,T_t(\boldsymbol{v}_j^n))]\Big\}\,, \\ T_0(\boldsymbol{v}_i^n)=\boldsymbol{v}_i^n\,,\ \log|\det\nabla_{\boldsymbol{v}}T_0(\boldsymbol{v}_i^n)|=0\,, \end{cases} \tag{20}$$

Then $\boldsymbol{v}_i^{n+1} := T_1^{n+1}(\boldsymbol{v}_i^n)$ and $f^{n+1} := T_1^{n+1}{}_\# f^n$.

The particle formulation (20) immediately has the following favorable properties.

Proposition 3.1. *The particle-based variational formulation* (20) *has the following properties for any $n \geq 0$:*

(i) Discrete entropy dissipation: $\frac{1}{N}\sum_{i=1}^N \log f^{n+1}(\boldsymbol{v}_i^{n+1}) \leq \frac{1}{N}\sum_{i=1}^N \log f^n(\boldsymbol{v}_i^n)$.

(ii) Discrete mass, momentum, and energy conservation: $\frac{1}{N}\sum_{i=1}^N \varphi(\boldsymbol{v}_i^{n+1}) = \frac{1}{N}\sum_{i=1}^N \varphi(\boldsymbol{v}_i^n)$, for $\varphi(\boldsymbol{v}) = 1\,, \boldsymbol{v}\,, |\boldsymbol{v}|^2$.

Proof. Property (i) is a direct consequence of optimization. Property (ii) is true thanks to the flow map constraint: for $\varphi(\boldsymbol{v}) = 1\,, \boldsymbol{v}\,, |\boldsymbol{v}|^2$, denote $\boldsymbol{v}_i^n(t) := T_t(\boldsymbol{v}_i^n)$, then

$$\begin{aligned} &\frac{\mathrm{d}}{\mathrm{d}t}\frac{1}{N}\sum_{i=1}^N\varphi(\boldsymbol{v}_i^n(t)) = \frac{1}{N}\sum_{i=1}^N\nabla\varphi(\boldsymbol{v}_i^n(t))\cdot\frac{\mathrm{d}}{\mathrm{d}t}\boldsymbol{v}_i^n(t) \\ =& -\frac{1}{N^2}\sum_{i=1}^N\sum_{j=1}^N\nabla\varphi(\boldsymbol{v}_i^n(t))\cdot A(\boldsymbol{v}_i^n(t)-\boldsymbol{v}_j^n(t))[\boldsymbol{u}(t,\boldsymbol{v}_i^n(t))-\boldsymbol{u}(t,\boldsymbol{v}_j^n(t))] \end{aligned}$$

$$= -\frac{1}{2N^2}\sum_{i=1}^N\sum_{j=1}^N[\nabla\varphi(\boldsymbol{v}_i^n(t)) - \nabla\varphi(\boldsymbol{v}_j^n(t))]\cdot A(\boldsymbol{v}_i^n(t) - \boldsymbol{v}_j^n(t))[\boldsymbol{u}(t, \boldsymbol{v}_i^n(t)) - \boldsymbol{u}(t, \boldsymbol{v}_j^n(t))] = 0\,.$$

□

At the fully discrete level, the inner time in the dynamic formulation is discretized using a one-step forward Euler method, making the vector field $\boldsymbol{u}$ independent of the inner time. Although higher-order ODE solvers such as RK4 could be used, the forward Euler method does not compromise the first-order accuracy of the original JKO scheme, as noted in [30, Theorem 3]. In practice, we replace $\boldsymbol{u}$ by $\tau\boldsymbol{u}$ (this is equivalent to changing the inner time from $[0, 1]$ to $[0, \tau]$), and finally arrive at the following problem:

$$\begin{cases} \boldsymbol{u}^{n+1} \in \arg\inf\limits_{\boldsymbol{u}} \; \dfrac{\tau^2}{2N^2}\displaystyle\sum_{i=1}^N\sum_{j=1}^N d_{i,j}^{n+1}(\boldsymbol{u}) + \dfrac{2\tau^2}{N^2}\displaystyle\sum_{i=1}^N\sum_{j=1}^N h_{i,j}^{n+1}(\boldsymbol{u})\,, \\ \text{where} \\ d_{i,j}^{n+1}(\boldsymbol{u}) = [\boldsymbol{u}(\boldsymbol{v}_i^n) - \boldsymbol{u}(\boldsymbol{v}_j^n)]\cdot A(\boldsymbol{v}_i^n - \boldsymbol{v}_j^n)[\boldsymbol{u}(\boldsymbol{v}_i^n) - \boldsymbol{u}(\boldsymbol{v}_j^n)]\,, \\ h_{i,j}^{n+1}(\boldsymbol{u}) = A(\boldsymbol{v}_i^n - \boldsymbol{v}_j^n) : \nabla\boldsymbol{u}(\boldsymbol{v}_i^n) - (d-1)C_\gamma|\boldsymbol{v}_i^n - \boldsymbol{v}_j^n|^\gamma(\boldsymbol{v}_i^n - \boldsymbol{v}_j^n)\cdot[\boldsymbol{u}(\boldsymbol{v}_i^n) - \boldsymbol{u}(\boldsymbol{v}_j^n)]\,. \end{cases} \tag{21}$$

Once $\boldsymbol{u}^{n+1}$ is obtained, we update velocity of particles and densities by

$$\boldsymbol{v}_i^{n+1} = \boldsymbol{v}_i^n - \frac{\tau}{N}\sum_{j=1}^N A(\boldsymbol{v}_i^n - \boldsymbol{v}_j^n)[\boldsymbol{u}^{n+1}(\boldsymbol{v}_i^n) - \boldsymbol{u}^{n+1}(\boldsymbol{v}_j^n)]\,, \tag{22}$$

$$h_i^{n+1}(\boldsymbol{u}^{n+1}) = -\frac{\tau}{N}\sum_{j=1}^N h_{i,j}^{n+1}(\boldsymbol{u}^{n+1})\,,\; f^{n+1}(\boldsymbol{v}_i^{n+1}) = \frac{f^n(\boldsymbol{v}_i^n)}{\exp(h_i^{n+1}(\boldsymbol{u}^{n+1}))}\,. \tag{23}$$

Proposition 3.2. *The variational particle method (21–23) has the following properties for any $n \geq 0$:*

(i) Discrete entropy dissipation: $\frac{1}{N}\sum_{i=1}^N \log f^{n+1}(\boldsymbol{v}_i^{n+1}) \leq \frac{1}{N}\sum_{i=1}^N \log f^n(\boldsymbol{v}_i^n)$.

(ii) Discrete mass and momentum conservation: $\frac{1}{N}\sum_{i=1}^N \varphi(\boldsymbol{v}_i^{n+1}) = \frac{1}{N}\sum_{i=1}^N \varphi(\boldsymbol{v}_i^n)$ for $\varphi(\boldsymbol{v}) = 1, \boldsymbol{v}$.

(iii) Discrete energy $\frac{1}{N}\sum_{i=1}^N |\boldsymbol{v}_i^n|^2$ is conserved up to $\mathcal{O}(\tau)$.

Proof. Property (i) is a direct consequence of optimization. Properties (ii) and (iii) are similar to the proof of [24, Proposition 2.3], so we omit it here. □

3.2 Neural network approximation

To implement (21), we need to represent the vector field $\boldsymbol{u}$. Representing it on the spatial grid leads to the curse of dimensionality. Instead, a more dimensionally agnostic representation is desirable. To achieve this, we use a neural network and denote the approximation as $\boldsymbol{u}_\theta$.

As noted earlier in (17), the optimal vector field takes the form of the score function $\nabla\log f$, with an additional term in *span*$\{\mathbf{1}, \boldsymbol{v}\}$. This additional term is negligible because, when multiplied by $A(\boldsymbol{v} - \boldsymbol{v}_*)$, it vanishes. Based on this observation, we initialize our neural network $\boldsymbol{u}_\theta^0$ close to the initial score function by minimizing the relative L^2 loss:

$$\ell^0(\theta) := \frac{\int_{\mathbb{R}^d}|\boldsymbol{u}_\theta^0(\boldsymbol{v}) - \nabla\log f^0(\boldsymbol{v})|^2 f^0(\boldsymbol{v})\mathrm{d}\boldsymbol{v}}{\int_{\mathbb{R}^d}|\nabla\log f^0(\boldsymbol{v})|^2 f^0(\boldsymbol{v})\mathrm{d}\boldsymbol{v}} \approx \frac{\sum_{i=1}^N|\boldsymbol{u}_\theta^0(\boldsymbol{v}_i^0) - \nabla\log f^0(\boldsymbol{v}_i^0)|^2}{\sum_{i=1}^N|\nabla\log f^0(\boldsymbol{v}_i^0)|^2}\,, \tag{24}$$

where $\{\boldsymbol{v}_i^0\}_{i=1}^N$ are sampled from the initial distribution f^0. In the subsequent steps ($n \geq 0$), we initialize $\boldsymbol{u}_\theta^{n+1}$ for the $n+1$–th JKO step from previously trained $\boldsymbol{u}_\theta^n$, which leads to improved performance and faster convergence. We then train $\boldsymbol{u}_\theta^{n+1}$ by minimizing the JKO loss (21) at the $n+1$–th JKO step:

$$\ell^{n+1}(\theta) = \frac{1}{N^2}\sum_{i=1}^N\sum_{j=1}^N \underbrace{\frac{\tau^2}{2}d_{i,j}^{n+1}(\boldsymbol{u}_\theta^{n+1}) + 2\tau^2 h_{i,j}^{n+1}(\boldsymbol{u}_\theta^{n+1})}_{=:\ell_{i,j}^{n+1}(\theta)}\,. \tag{25}$$

Once the neural network $\boldsymbol{u}_\theta^{n+1}$ is learned, we update the velocity of particles and density along particle trajectories by equations (22–23). The procedure of the JKO-based particle method is summarized in Algorithm 1.

Algorithm 1 JKO-based particle method for homogeneous Landau equation

```
Input: $N$ initial particles $\{\boldsymbol{v}_i^0\}_{i=1}^N \overset{i.i.d.}{\sim} f^0$; JKO time step $\tau$ and total number of JKO steps $N_T$.
Output: Neural networks $\boldsymbol{u}_\theta^n$, velocity of particles $\{\boldsymbol{v}_i^n\}_{i=1}^N$ and densities $\{f^n(\boldsymbol{v}_i^n)\}_{i=1}^N$ for all $n = 1, \cdots, N_T$.
 1: Initialize neural network $\boldsymbol{u}_\theta^0$ by minimizing $\ell^0$ (24).
 2: for $n = 0, \cdots, N_T - 1$ do
 3:     Initialize neural network $\boldsymbol{u}_\theta^{n+1}$ from the previously trained $\boldsymbol{u}_\theta^n$.
 4:     while not converged do
 5:         Update $\theta$ of $\boldsymbol{u}_\theta^{n+1}$ by minimizing the JKO loss $\ell^{n+1}$ (25) using Algorithm 2.
 6:     end while
 7:     for $i = 1, \cdots, N$ do
 8:         obtain $\boldsymbol{v}_i^{n+1}$ from $\boldsymbol{v}_i^n$ and $f^{n+1}(\boldsymbol{v}_i^{n+1})$ from $f^n(\boldsymbol{v}_i^n)$ via (22–23).
 9:     end for
10: end for
```

4 Stochasticity accelerated JKO scheme

One advantage of (21) is that it is well-suited for stochastic methods, which are crucial for high-dimensional problems due to their efficiency and reduced memory consumption. In this section, we provide a detailed discussion on leveraging stochasticity in optimization and examine its convergence. Once $\boldsymbol{u}$ is learned, particle updates can also be accelerated using the random batch method [26], with further details provided in Section 4.3.

4.1 Stochastic optimization

Comparing the proposed JKO-based method with the score-based method [24, 25], the primary difference lies in their loss functions. The JKO loss function is designed to respect entropy dissipation, which therefore has exact entropy decay and unconditional stability. However, this comes at the cost of a more complex loss function. Specifically, the loss function in the score-based method takes the form:

$$\frac{1}{N}\sum_{i=1}^N |\boldsymbol{u}_\theta^n(\boldsymbol{v}_i^n)|^2 + 2\nabla\cdot\boldsymbol{u}_\theta^n(\boldsymbol{v}_i^n)\,, \tag{26}$$

which is significantly simpler than (21). In particular, (26) involves only a single summation, resulting in $\mathcal{O}(N)$ computational complexity, whereas (21) involves a double sum, leading to $\mathcal{O}(N^2)$ complexity. Additionally, when implementing it in parallel, (21) encounters issues like the GPU out-of-memory error when N gets large.

Nevertheless, a common approach to address these issues is to apply stochastic optimization algorithms, such as the standard mini-batch SGD [4]. In this method, indices i and j are treated as independent, and a batch of index pairs $(i, j) \in [N] \times [N]$ is randomly selected to perform the gradient computation. However, in our case, i and j represent two interacting particles, and they interact through elastic collisions. Therefore, it is crucial to preserve their relationship. To address this, we first randomly select a batch of indices from $[N]$ and then update parameter θ based on the gradient information within this batch.

To further speed up the training process, we adopt the shuffling-type gradient method [31]. That is, for each epoch, we choose a batch size B ($B \ll N$) and randomly divide N indices into $\frac{N}{B}$ batches, denoted by C_q, $q = 1, \ldots, \frac{N}{B}$. We then perform one step of gradient descent within each C_q successively. Thus the cost of one gradient descent decreases to $\mathcal{O}(BN)$. The random division can be realized in $\mathcal{O}(N)$ through random permutation, via PyTorch function such as 'torch.utils.data.DataLoader'. Consequently, the total computational cost per epoch is significantly reduced to $\mathcal{O}(N)$. In practice, the batch size is chosen heuristically to balance accuracy and computational time, and the basic gradient descent is substituted with more efficient optimizers like `Adamax`. The procedure is summarized in Algorithm 2, with the time subscript omitted for simplicity.

4.2 Convergence analysis for optimization

Following the analysis of the SGD with random reshuffling [31], in this section we show the convergence of Algorithm 2. Recall the definition of $l(\theta)$ and $l_{i,j}(\theta)$, we first make the following assumptions, which are standard in optimization theory.

(A.1) *dom*$(\ell) := \{\theta \in \mathbb{R}^{d_\theta} : \ell(\theta) < +\infty\} \neq \emptyset$ and $\ell_* := \inf_\theta \ell(\theta) > -\infty$.

(A.2) $\ell_{i,j}(\theta)$ is L-smooth, i.e. $\|\nabla_\theta \ell_{i,j}(\theta_2) - \nabla_\theta \ell_{i,j}(\theta_1)\| \le L\|\theta_2 - \theta_1\|$, for all $i, j \in [N]$.

(A.3) $\nabla l_{i,j}$ has bounded variance: $\exists$ two constants $M \ge 0$ and $\sigma > 0$ such that for all $\theta \in \mathbb{R}^{d_\theta}$, we have $\frac{1}{N^2}\sum_{i=1}^N\sum_{j=1}^N \|\nabla\ell_{i,j}(\theta) - \nabla\ell(\theta)\|^2 \le M\,\|\nabla\ell(\theta)\|^2 + \sigma^2\,.$

Algorithm 2 mini-batch SGD with random reshuffling

```
Input: Initial parameters $\theta_0$; mini-batch size $B$; epoch numbers $K$.
Output: Trained parameters $\theta_K$.
1: for epoch $k = 1, \cdots, K$ do
2:     Set $\theta_0^{(k)} = \theta_{k-1}$.
3:     Divide $N$ into $\frac{N}{B}$ batches denoted by $C_q$ with size $B$ randomly.
4:     for $q = 1, \dots, \frac{N}{B}$ do
5:         $\theta_q^{(k)} = \theta_{q-1}^{(k)} - \alpha_q^{(k)} \frac{1}{B^2} \sum_{i,j \in C_q} \nabla_\theta \ell_{i,j}(\theta_{q-1}^{(k)})$
6:     end for
7:     Set $\theta_k = \theta_{\frac{N}{B}}^{(k)}$.
8: end for
```

The main result is as follows.

Theorem 4.1. *Suppose the above assumptions hold. Let learning rate $\alpha_q^{(k)} := \alpha \frac{B}{N} > 0$ for $0 < \alpha \le \frac{1}{L\sqrt{2(3M+2)}} \frac{B}{N}$. Then after K epochs we have,*

$$\frac{1}{K} \sum_{k=0}^{K-1} \mathbb{E}\left[\|\nabla_\theta \ell(\theta_k)\|^2\right] \le \frac{4}{\alpha K}\left[\ell(\theta_0) - \ell_*\right] + 6\sigma^2 L^2 \alpha^2 \frac{N}{B^2}.$$

As mentioned earlier, the main difference between our method with the vanilla mini-batch SGD is the treatment of the indices i and j. Consequently, the corresponding gradient needs to estimated differently.

Proof. Combining Lemma B.1 and B.2, we have

$$\begin{aligned} \ell(\theta_{k+1}) &\le \ell(\theta_k) + \frac{\alpha L^2 B}{2N} \sum_{q=1}^{\frac{N}{B}} \left\|\theta_k - \theta_{q-1}^{(k+1)}\right\|^2 - \frac{\alpha}{2}\|\nabla \ell(\theta_k)\|^2 \\ &\le \ell(\theta_k) + \frac{\alpha L^2}{2N} \frac{\alpha^2 N^2}{B^2}\left((3M+2)\|\nabla_\theta \ell(\theta_k)\|^2 + 3\sigma^2\right) - \frac{\alpha}{2}\|\nabla \ell(\theta_k)\|^2 \\ &= \ell(\theta_k) + \frac{\alpha}{2}\left(\frac{\alpha^2 L^2 N}{B^2}(3M+2) - 1\right)\|\nabla_\theta \ell(\theta_k)\|^2 + \frac{3\alpha_k^3 \sigma^2 L^2 N}{2B^2}. \end{aligned}$$

Since $0 < \alpha \le \frac{1}{L\sqrt{2(3M+2)}} \frac{B}{N}$, we have $\frac{\alpha^2 L^2 N}{B^2}(3M+2) - 1 \le -\frac{1}{2}$. Hence,

$$\ell(\theta_{k+1}) \le \ell(\theta_k) - \frac{\alpha}{4}\|\nabla_\theta \ell(\theta_k)\|^2 + \frac{3\sigma^2 L^2}{2} \frac{\alpha^3 N}{B^2}.$$

Rearranging the above inequality, we see that

$$\begin{aligned} \frac{1}{K} \sum_{k=0}^{K-1} \|\nabla_\theta \ell(\theta_k)\|^2 &\le \frac{4}{\alpha K} \sum_{k=0}^{K-1} [\ell(\theta_k) - \ell(\theta_{k+1})] + 6\sigma^2 L^2 \alpha^2 \frac{N}{B^2} \\ &= \frac{4}{\alpha K}[\ell(\theta_0) - \ell(\theta_K)] + 6\sigma^2 L^2 \alpha^2 \frac{N}{B^2} \\ &\le \frac{4}{\alpha K}[\ell(\theta_0) - \ell_*] + 6\sigma^2 L^2 \alpha^2 \frac{N}{B^2}. \end{aligned}$$

The final result is obtained by taking the expectation. □

4.3 Random batch method

Utilizing the update equation (22–23) with full particles can be computationally expensive when particle number gets large or in high dimensions. The random batch method [26, 9] is designed to address this challenge by restricting particle collisions to small, randomly selected batches. This is what we will adopt here.

Given N particles, we randomly divide them into $\frac{N}{B'}$ batches C_q, $q = 1, \dots, \frac{N}{B'}$, with a batch size $B' \ll N$. For i–th particle in batch C_q, we update it using the following equation:

$$\boldsymbol{v}_i^{n+1} = \boldsymbol{v}_i^n - \frac{\tau}{B'} \sum_{j \in C_q} A(\boldsymbol{v}_i^n - \boldsymbol{v}_j^n)[\boldsymbol{u}_\theta^{n+1}(\boldsymbol{v}_i^n) - \boldsymbol{u}_\theta^{n+1}(\boldsymbol{v}_j^n)],$$

$$h_i^{n+1}(\boldsymbol{u}_\theta^{n+1}) = -\frac{\tau}{B'} \sum_{j \in C_q} h_{i,j}^{n+1}(\boldsymbol{u}_\theta^{n+1}), \quad f^{n+1}(\boldsymbol{v}_i^{n+1}) = \frac{f^n(\boldsymbol{v}_i^n)}{\exp\left(h_i^{n+1}(\boldsymbol{u}_\theta^{n+1})\right)}.$$

Since each particle interacts only within its own batch, the complexity of updating particles reduces from $\mathcal{O}(N^2)$ to $\mathcal{O}(B'N)$ per JKO step. This approach accelerates the particle updates and preserves all physical quantities without significantly impacting the accuracy, as demonstrated in [26, 9].

5 Numerical examples

In this section, we present several numerical examples using the proposed JKO-based particle method, covering both Maxwellian and Coulomb cases. To visualize particle density and compare it with the reference solution, we either use kernel density estimation with Gaussian kernel ψ_ε:

$$f^n_{kde}(\boldsymbol{v}) := \frac{1}{N}\sum_{i=1}^{N}\psi_\varepsilon(\boldsymbol{v}-\boldsymbol{v}_i^n)\,, \;\; \psi_\varepsilon(\boldsymbol{v}) = \frac{1}{(2\pi\varepsilon^2)^{d/2}}\exp\left(-\frac{|\boldsymbol{v}|^2}{2\varepsilon^2}\right); \tag{27}$$

or through density update equation (23), which enables us to directly obtain the density from those evolved particles.

Throughout the examples, unless otherwise specified, the vector field $\boldsymbol{u}$ is parameterized as a fully-connected neural network with 3 hidden layers, each containing 32 neurons, and the `swish` activation function. The biases in the hidden layers are initialized to zero, while the weights are initialized using a truncated normal distribution with a variance of 1/`fan_in`. Training is performed using the `Adamax` optimizer.

5.1 2D BKW solution for Maxwellian molecules

We first evaluate the accuracy of our method using the BKW solution to the Landau equation (see [8, Appendix A]), which has an analytical expression and thus serves as an excellent benchmark for accuracy verification. Specifically, in two dimensions, consider the collision kernel $A(\boldsymbol{z}) = \frac{1}{16}(|\boldsymbol{z}|^2 I_2 - \boldsymbol{z}\otimes\boldsymbol{z})$, then the BKW solution takes the form:

$$f(t,\boldsymbol{v}) = \frac{1}{2\pi K}\exp\left(-\frac{|\boldsymbol{v}|^2}{2K}\right)\left(\frac{2K-1}{K}+\frac{1-K}{2K^2}|\boldsymbol{v}|^2\right)\,,\; K = 1-\frac{1}{2}\exp\left(-\frac{t}{8}\right). \tag{28}$$

In the numerical experiment, we set the JKO time step to $\tau = 0.01$. The total number of particles are set to $N = 160^2$, initially i.i.d. sampled from the initial distribution using rejection sampling. The learning rate is chosen to be $\alpha = 2\times 10^{-4}$ for $t \le 2.5$, and $\alpha = 10^{-4}$ thereafter. The number of epochs is set to 3 for each JKO step, and the batch size is 1280.

Fig. 1 illustrates the conservation and the entropy dissipation properties of our solver. On the left, the kinetic energy is conserved with only a small error. In the center, the entropy closely matches the analytical value (computed using quadrature rule on a fine mesh). On the right, we observe that the entropy converges exponentially fast to equilibrium, in line with the theoretical results from [34].

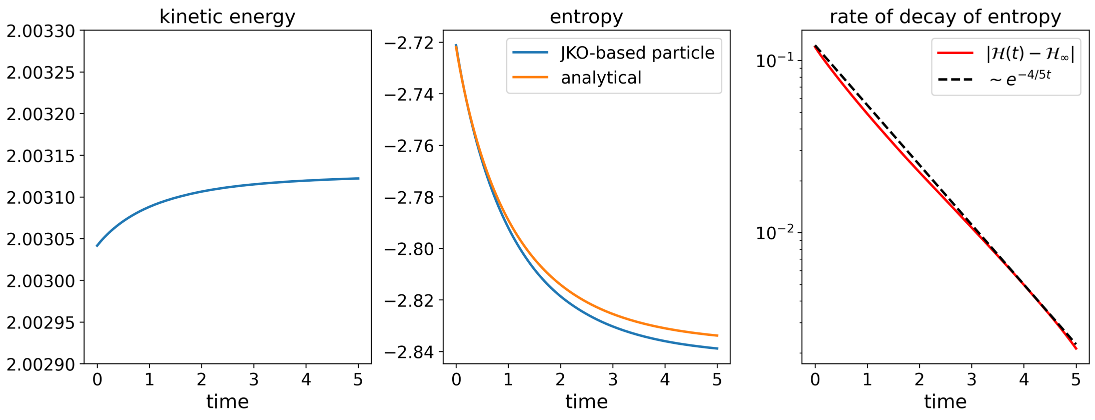

Figure 1: Time evolution of macroscopical physical quantities for a 2D BKW solution. Left: time evolution of the kinetic energy, where the exact kinetic energy is 2. Center: time evolution of the entropy. Right: rate of decay of entropy with respect to time.

In Fig. 2, we present scatter plots of the particles at $t = 0, 1$, and 5. In each plot, the color of the particles corresponds to the density values, with brighter colors indicating higher densities. The density is either computed using the exact formula (28) (top row) or the density formula (23) (bottom row). For a quantitative comparison, Fig. 3 shows the relative error L^2-error defined by

$$\frac{\sqrt{\sum_{z=1}^{Z} |f_{kde}^n(\boldsymbol{v}_z^c) - f_{exact}^n(\boldsymbol{v}_z^c)|^2}}{\sqrt{\sum_{z=1}^{Z} |f_{exact}^n(\boldsymbol{v}_z^c)|^2}} \tag{29}$$

over time. Here f_{kde}^n denotes the densities reconstructed by the kernel density estimation (27) with $\varepsilon = 0.15$. The evaluation grids $\boldsymbol{v}_z^c$ consist of $Z = 100^2$ equidistant points over the computational domain $[-4, 4]^2$.

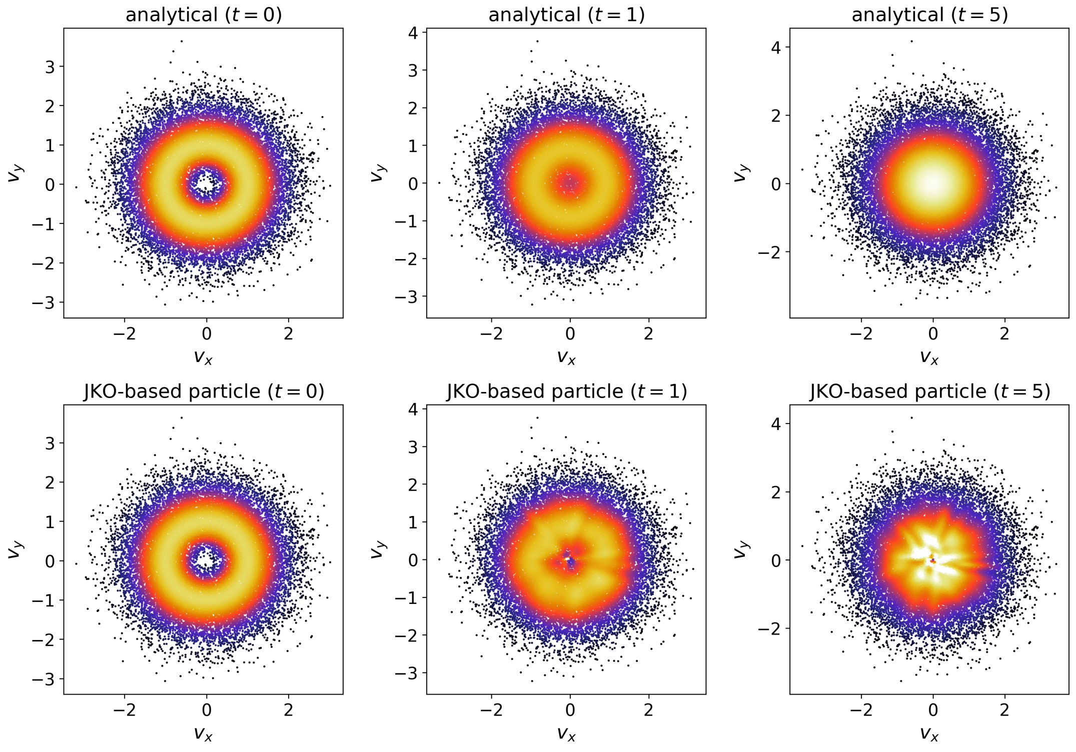

Figure 2: Scatter plots for a 2D BKW solution at $t = 0, 1$, and 5. Top: analytical solution. Bottom: particle solution.

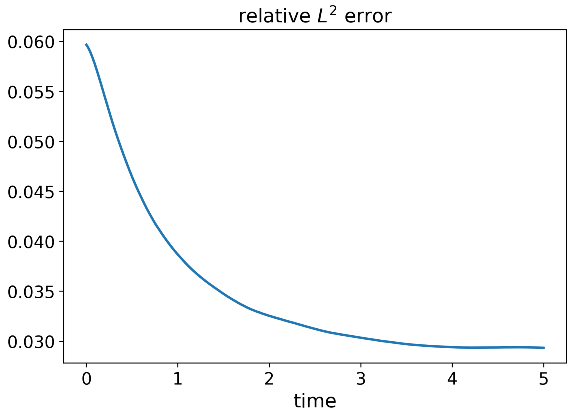

Figure 3: Time evolution of the relative L^2-error (29) between the reconstructed and analytical solution for a 2D BKW solution.

5.2 3D BKW solution for Maxwellian molecules

In three dimensions, the BKW solution corresponding to the collision kernel $A(\boldsymbol{z}) = \frac{1}{24}(|\boldsymbol{z}|^2 I_3 - \boldsymbol{z} \otimes \boldsymbol{z})$ reads:

$$f(t, \boldsymbol{v}) = \frac{1}{(2\pi K)^{3/2}} \exp\left(-\frac{|\boldsymbol{v}|^2}{2K}\right)\left(\frac{5K-3}{2K} + \frac{1-K}{2K^2}|\boldsymbol{v}|^2\right), \; K = 1 - \exp\left(-\frac{t}{6}\right).$$

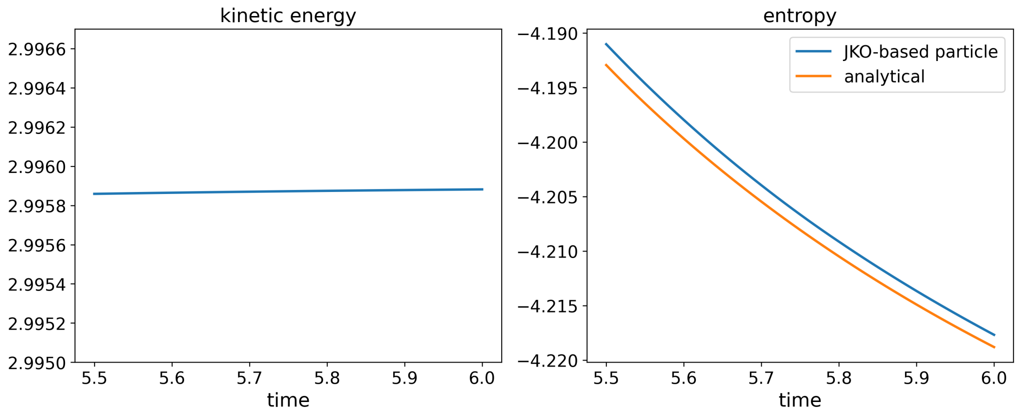

Figure 4: Time evolution of macroscopical physical quantities for a 3D BKW solution. Left: time evolution of the kinetic energy, where the exact kinetic energy is 3. Right: time evolution of the entropy.

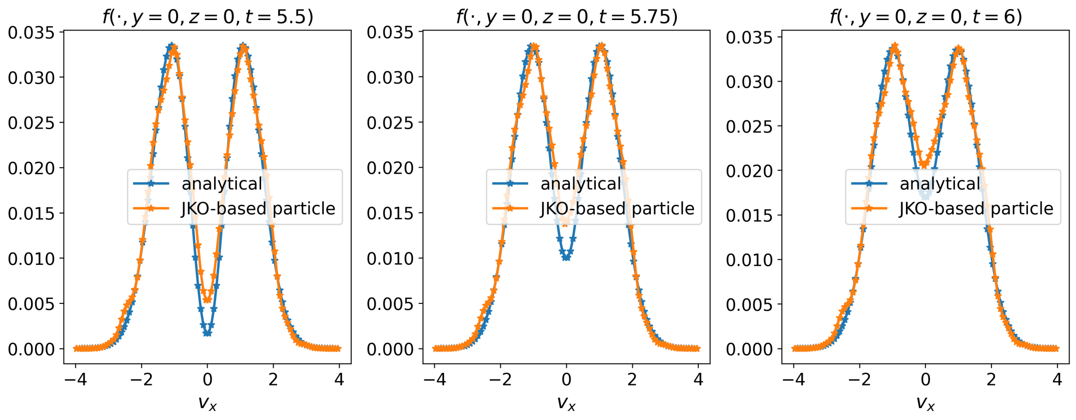

Figure 5: Slice plots of $f(\cdot, y=0, z=0)$ of the reconstructed and analytical solution for a 3D BKW solution at $t = 5.5$, 5.75, and 6.

Here, we set the JKO time step to $\tau = 0.01$ and the total number of particles to $N = 40^3$. The learning rate is $\alpha = 10^{-4}$, the number of epochs is set to 5 for each JKO step, and the batch size is 640.

As shown in Fig. 4, our solution conserves kinetic energy (up to τ) and closely matches the analytical entropy. In Fig. 5, we plot slices of the reconstructed solution on the computational domain $[-4,4]^3$ at $t = 5$, 5.75, and 6. The Gaussian kernel bandwidth is set to $\varepsilon = 0.15$.

5.3 2D bi-Maxwellian example with Coulomb interaction

Now we consider a more physically relevant interaction: the Coulomb interaction. First, let us examine the two-dimensional case, where the collision kernel is $A(\boldsymbol{z}) = \frac{1}{16}\frac{1}{|\boldsymbol{z}|^3}(|\boldsymbol{z}|^2 I_2 - \boldsymbol{z} \otimes \boldsymbol{z})$. We choose an initial distribution given by a bi-Maxwellian:

$$f^0(\boldsymbol{v}) = \frac{1}{4\pi}\left\{\exp\left(-\frac{|\boldsymbol{v}-\boldsymbol{v}_1|^2}{2}\right) + \exp\left(-\frac{|\boldsymbol{v}-\boldsymbol{v}_2|^2}{2}\right)\right\}, \;\boldsymbol{v}_1 = (-2,1),\;\boldsymbol{v}_2 = (0,-1)\,.$$

In this test, the numerical parameters are set as follows: the JKO time step is $\tau = 0.1$, the total number of particles is $N = 120^2$, the learning rate is $\alpha = 10^{-4}$ for $t \leq 80$, and $\alpha = 5 \times 10^{-5}$ thereafter, the number of epochs is 3 for each JKO step, and the batch size is 900.

Since there is no analytical solution for this example, we compare our solution with the blob solution obtained using the deterministic particle method from [8], with the same number of particles. We set the computational domain to $[-10,10]^2$ and use a Gaussian kernel with bandwidth $\varepsilon = 0.3$ for density computation. The similarity between the reconstructed solution and the blob solution, as shown in Fig. 6, indicates that the JKO-based particle method is effective for Coulomb interactions. Fig. 7 demonstrates that our method conserves energy and maintains entropy dissipation reasonably well. Additionally, Fig. 8 depicts the evolution of the particle solution from $t = 0$ to $t = 160$, showing the transition from the initial bi-Maxwellian distribution to the equilibrium Maxwellian distribution.

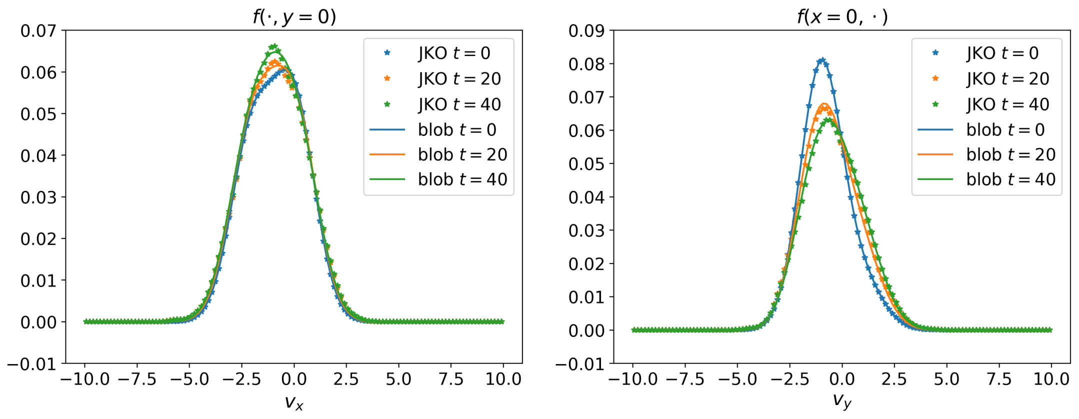

Figure 6: Slices of the reconstructed and blob solution for an example of 2D Coulomb interaction at $t = 0$, 20, and 40. Left: $f(\cdot, y = 0)$. Right: $f(x = 0, \cdot)$.

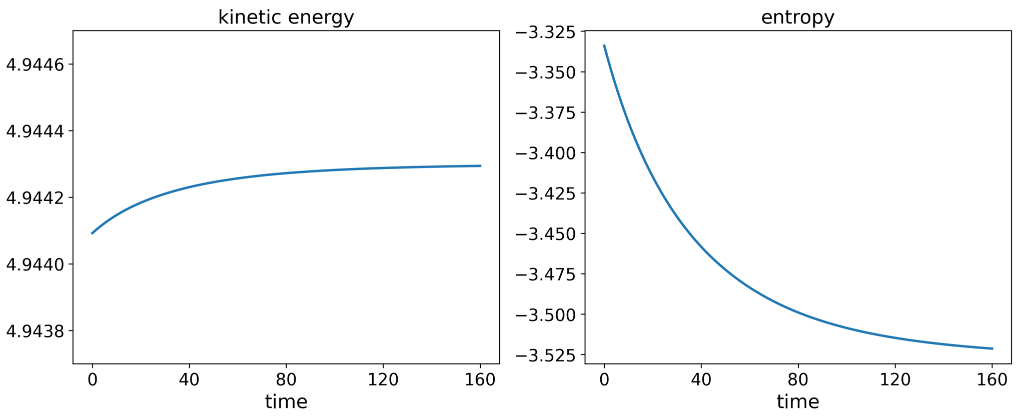

Figure 7: Time evolution of macroscopic physical quantities for an example of 2D Coulomb interaction. Left: time evolution of the kinetic energy, where the exact kinetic energy is 5. Right: time evolution of the entropy.

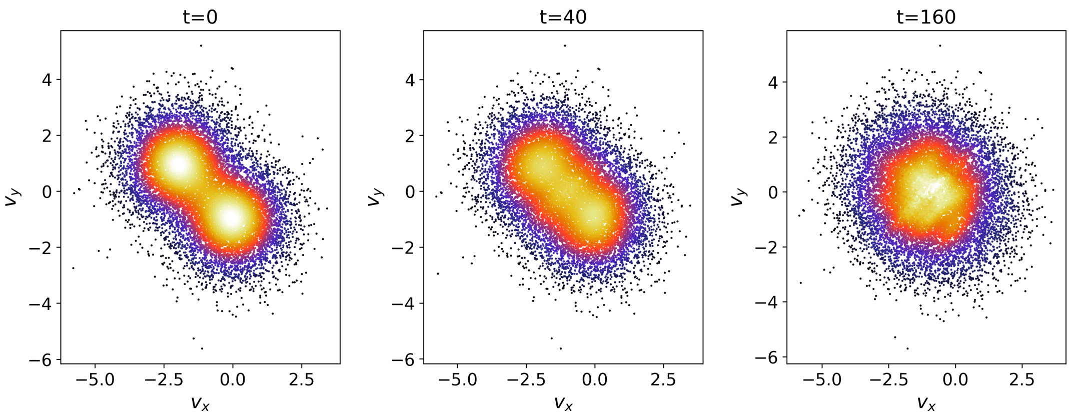

Figure 8: Scatter plots of particle solution for an example of 2D Coulomb interaction at $t = 0$, 40, and 160.

5.4 3D Rosenbluth problem with Coulomb interaction

Here, we extend our consideration of Coulomb interactions to three dimensions, using the collision kernel given by: $A(\boldsymbol{z}) = \frac{1}{4\pi}\frac{1}{|\boldsymbol{z}|^3}(|\boldsymbol{z}|^2 I_3 - \boldsymbol{z}\otimes\boldsymbol{z})$. The initial condition is set to

$$f^0(\boldsymbol{v}) = \frac{1}{S^2}\exp\left(-S\frac{(|\boldsymbol{v}|-\sigma)^2}{\sigma^2}\right)\,,\ \sigma = 0.3\,,\ S = 10\,.$$

We solve this problem using a JKO time step of $\tau = 0.2$, with a total of $N = 50^3$ particles. The neural network for vector field $\boldsymbol{u}$ is a residue neural network [23] configured with 3 hidden layers, 32 neurons per hidden layer, and `swish` activation function, and initialized identically to the first example. The learning rate is $\alpha = 10^{-4}$ for $t \leq 10$, and $\alpha = 5\times 10^{-5}$ thereafter. We use 3 epochs for each JKO step, with a batch size of 640. Additionally, a random batch method with a batch size of 1280 is employed for particle updates.

In Fig. 9, we show the density reconstructed using kernel density estimation (27) with $\varepsilon = 0.035$. The result is in good agreement with the solutions presented in [8].

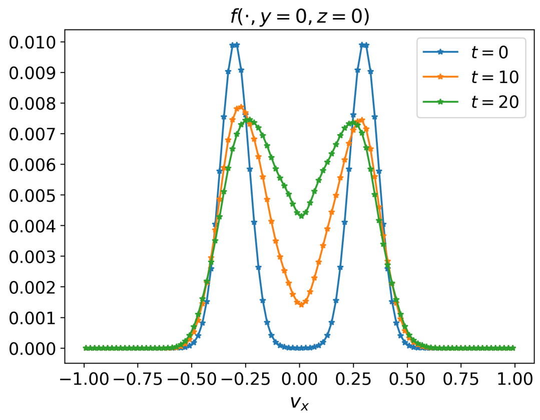

Figure 9: Slices $f(\cdot, y = 0, z = 0)$ of the reconstructed solution for a 3D Rosenbluth problem with Coulomb interaction at $t = 0$, 10, and 20.

To demonstrate the effectiveness of our JKO-based method in capturing equilibrium, we conducted experiments using relatively large time steps, $\tau = 1$ and $\tau = 5$, up to time $t = 500$, with a total of $N = 25600$ particles. The results, shown in Fig. 10, indicate that our method remains stable despite the large time step size and that the entropy approaches equilibrium effectively. Here, the equilibrium Maxwellian distribution is given by $\frac{\rho}{(2\pi T)^{d/2}}\exp\left(-\frac{|\boldsymbol{v}|^2}{2T}\right)$ with

$$\rho = \frac{2\pi\sigma^3}{S^2}\left[\left(1+\frac{1}{2S}\right)\sqrt{\frac{\pi}{S}}\mathrm{erfc}(-\sqrt{S}) + \frac{1}{S}\exp(-S)\right]\,,$$
$$T = \frac{2\pi\sigma^5}{3\rho S^2}\left[\left(1+\frac{3}{S}+\frac{3}{4S^2}\right)\sqrt{\frac{\pi}{S}}\mathrm{erfc}(-\sqrt{S}) + \left(\frac{1}{S}+\frac{5}{2S^2}\right)\exp(-S)\right]\,,$$

and the equilibrium entropy is $\mathcal{H}_\infty = \rho\log\rho - \frac{3}{2}\rho\log(2\pi e T)$.

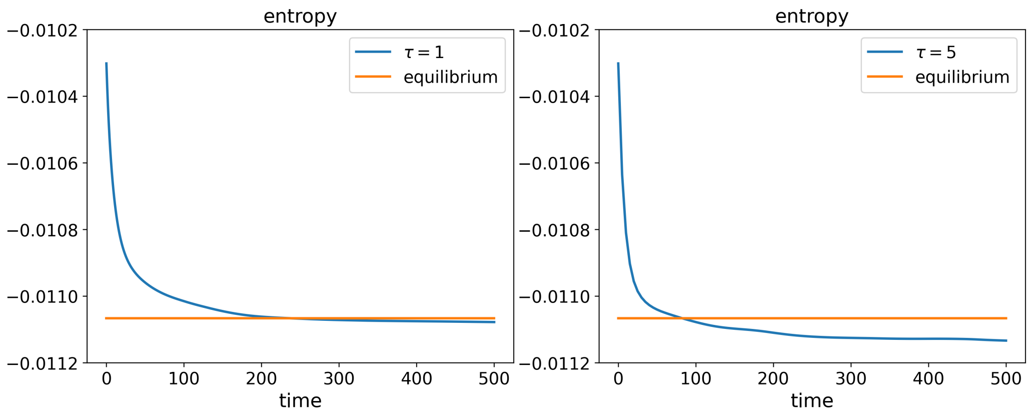

Figure 10: Time evolution of entropy for a 3D Rosenbluth problem with Coulomb interaction. Left: JKO time step $\tau = 1$. Right: JKO time step $\tau = 5$.

We also use this example to test the computational efficiency of the proposed method in comparison with two other siblings: the deterministic particle method [8] and the score-based particle method [24]. The primary distinction among these methods lies in their approach to computing the score, i.e., $\nabla \log f$. Specifically, the deterministic particle method uses kernel density estimation to compute the score, the score-based method directly learns the score using the score-matching technique, and the JKO-based method optimizes to learn $\boldsymbol{u}$, and the optimizer turns out to be the score. To ensure a fair comparison, all the codes are written in PyTorch and executed on the Minnesota Supercomputer Institute Nvidia A40 GPU.

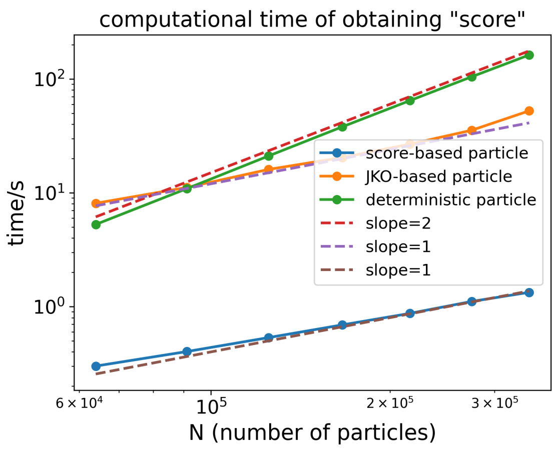

Figure 11: Comparison of the computational time (in seconds) for obtaining the "score" function using the deterministic, score-based, and JKO-based particle method on GPU.

As shown in Fig. 11, both the score-based and JKO-based method scales as $\mathcal{O}(N)$, with the score-based method being faster. This is expected, as both approaches involve learning the score through neural network training, but the score-based method has a simpler loss function. However, the JKO-based method offers additional benefits not shared with the score-based method, such as unconditional stability and exact entropy decay. In contrast, the deterministic particle method scales as $\mathcal{O}(N^2)$. It is important to emphasize that the reduction from $\mathcal{O}(N^2)$ to $\mathcal{O}(N)$ is significant, especially in higher dimensions, such as in the spatially inhomogeneous Landau equation, where the density exists in a six-dimensional phase space.

5.5 10D anisotropic solution with Maxwellian molecules

In real plasma simulations, the density f lives in a six-dimensional phase space, with three dimensions corresponding to spatial coordinates and three to velocity components. This high dimensionality presents a significant computational challenge. In this test, we aim to demonstrate the potential of our proposed method in managing such high-dimensional problems, leveraging the use of particles and neural networks for approximation. The example we use is adapted from [25, Example 5.3].

Consider the Maxwellian collision kernel $A(\boldsymbol{z}) = |\boldsymbol{z}|^2 I_d - \boldsymbol{z} \otimes \boldsymbol{z}$, and set the initial distribution as a normal distribution with zero mean and covariance $P_{i,j} = \delta_{i,j} p_i\,, p_1 = 1.8\,, p_2 = 0.2\,, p_i = 1\,, i = 3, \ldots, d$. In this case, there is no explicit formula for the density, but there is one for covariance matrix (stress tensor), $P(t) = \int_{\mathbb{R}^d} \boldsymbol{v} \otimes \boldsymbol{v} f(t, \boldsymbol{v}) \mathrm{d}\boldsymbol{v}$, as shown in [34]:

$$P_{i,j}(t) = P_{i,j}(\infty) - (P_{i,j}(\infty) - P_{i,j}(0))e^{-4dt}\,,\ P_{i,j}(\infty) = \frac{E}{d}\delta_{i,j}\,,\ E = \int_{\mathbb{R}^d} |\boldsymbol{v}|^2 f \mathrm{d}\boldsymbol{v}\,.$$

In our test, we consider a dimension of $d = 10$ and set the JKO time step size to $\tau = 0.002$, using a total of $N = 25600$ particles. We employ a fully connected neural network with 3 hidden layers, 128 neurons per layer, and the `swish` activation function to approximate the vector field $\boldsymbol{u}$. The initialization is as described at the beginning of this section. The learning rate is set to $\alpha = 10^{-4}$. We use 3 epochs for each JKO step, with a batch size of 640. Additionally, we use the random batch method with a batch size of 1280 for particle updates.

To examine the accuracy of our method, we compare the numerical covariance using particles $P^N_{i,j}(t^n) = \frac{1}{N}\sum_{k=1}^N (\boldsymbol{v}^n_k)_i (\boldsymbol{v}^n_k)_j$ with the analytical solution. Fig. 12 plots the time evolution of selected diagonal elements of the numerical covariance, which closely matches the analytical covariance. Additionally, we compute the Frobenius norm between the numerical and analytical covariances, $\sqrt{\sum_{i,j=1}^N (P^N_{i,j} - P_{i,j})^2}$, and the results are presented in Fig. 13. On the left, we show the time evolution of the Frobenius error with a fixed particle number $N = 25600$, which remains small throughout the experiment. On the right, we track the rate of convergence of the Frobenius error with respect to particle number at a fixed time $t = 0.1$. We observe that the convergence rate is slightly faster than the expected Monte Carlo convergence rate of $-\frac{1}{2}$, which is independent of the dimension.

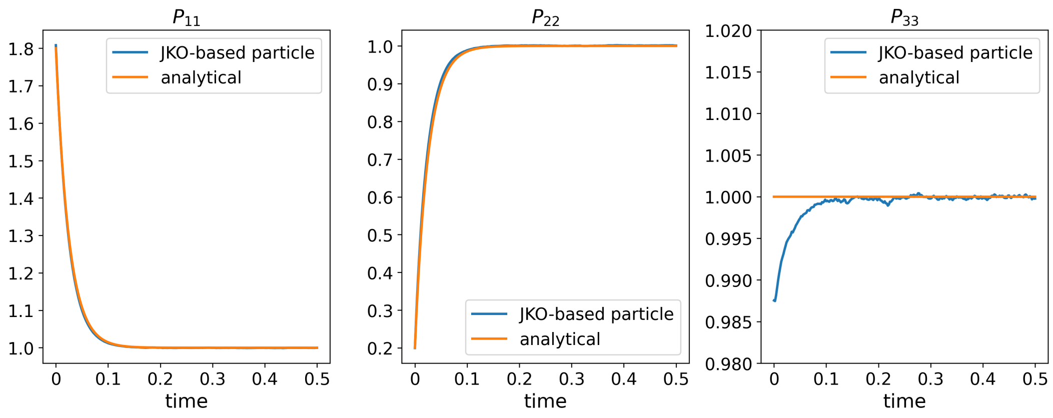

Figure 12: Time evolution of the first to third diagonal elements of the covariance matrix for the 10-D example.

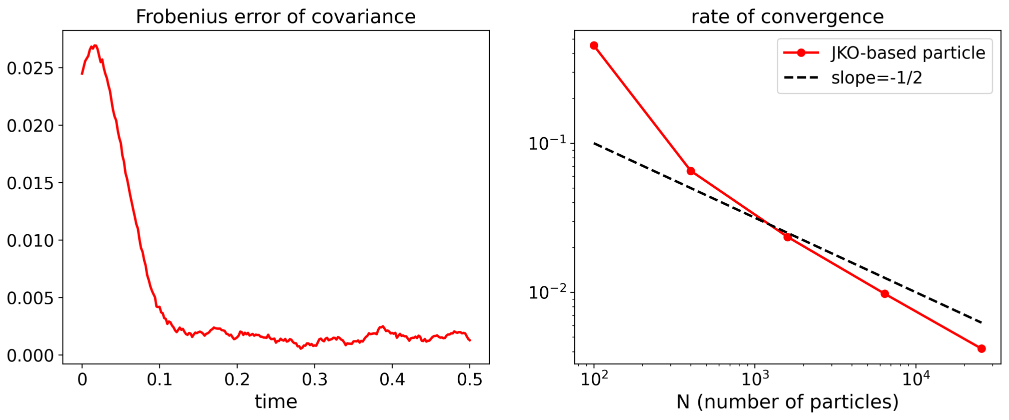

Figure 13: Error in covariance for the 10-D example. Left: Frobenius error versus time with fixed particle number $N = 25600$. Right: rate of convergence of the Frobenius error with respect to particle numbers at a fixed time $t = 0.1$.

6 Conclusion and discussion

In this paper, we design a neural network-based variational particle method for solving the homogeneous Landau equation, leveraging the underlying gradient flow structure. To address the complexity of the Landau metric, our main contributions include reformulating it into a form that can be easily represented by particles and recognizing that the unknown part is simply a score function of the corresponding density. These key insights provide essential guidance for neural network approximation and initialization. It is important to note that the objective function, when represented using particles, is in the form of double summation, which motivates us to design a tailored mini-batch stochastic optimization method. The particle update is further accelerated using the random batch method.

We have demonstrated that, compared to recent score-based particle methods for the Landau equation [24, 25], our approach involves a more complex objective function. However, this complexity is significantly mitigated by the use of stochastic methods. Additionally, our method offers unique advantages that the score-based method does not, including exact entropy decay and unconditional stability. When combined with the particle-in-cell method [19, 12, 2], these features make our approach promising for large-scale long time plasma simulations.

A Review of general gradient flow theory

We recall some important definitions of gradient flow on metric spaces that can be found in the Chapter 1 of [1]. Throughout this section, we consider the complete metric space (X, d) and the proper extended real functional $\varphi : X \to (-\infty, +\infty]$.

Definition 2 (Absolutely continuous curves). *A curve $\mu : (a,b) \to X$ is said to be an absolutely continuous curve if there exists $m \in L^2(a,b)$ such that $d(\mu_s, \mu_t) \leq \int_s^t m(r)\mathrm{d}r$, for $\forall a < s \leq t < b$.*

Definition 3 (Metric derivative). *For any absolutely continuous curve $\mu : (a,b) \to X$, the limit $|\mu'|(t) := \lim_{s\to t} \frac{d(\mu(s),\mu(t))}{|s-t|}$, exists for a.e. $t \in (a,b)$, and we define the limit as metric derivative of μ at t.*

Definition 4 (Strong upper gradients). *A function $g : X \to [0, +\infty]$ is a strong upper gradient for φ if for every absolutely continuous curve $\mu : (a,b) \to X$, the function $g \circ \mu$ is Borel and $|\varphi(\mu_t) - \varphi(\mu_s)| \leq \int_s^t g(\mu_r)|\mu'|(r)\mathrm{d}r$, for $\forall a < s \leq t < b$.*

Definition 5 (Curves of maximal slope). *An absolutely continuous curve $\mu : (a,b) \to X$ is said to be a curve of maximal slope for φ with respect to its strong upper gradient g, if $\varphi \circ \mu$ is equal to a non-increasing map a.e. in (a,b) and*

$$\varphi(\mu_t) - \varphi(\mu_s) + \frac{1}{2}\int_s^t g(\mu_r)^2\mathrm{d}r + \frac{1}{2}\int_s^t |\mu'|^2(r)\mathrm{d}r \leq 0\,,\ \forall a < s \leq t < b\,.$$

Note that the above inequality is indeed an equality by applying Young's inequality in the definition of the strong upper gradient.

B Lemmas for Theorem 4.1

Lemma B.1. *Suppose that assumptions (A.2) and (A.3) hold. Let learning rate $\alpha_q^{(k)} := \alpha_k \frac{B}{N} > 0$ for a given sequence $\{\alpha_k\}$ such that $0 < \alpha_k \leq \frac{1}{L\sqrt{3}}$. Then we have*

$$\Delta := \sum_{q=1}^{\frac{N}{B}} \left\|\theta_{q-1}^{(k)} - \theta_0^{(k)}\right\|^2 \leq \frac{\alpha_k^2 N^2}{B^2}\left((3M+2)\left\|\nabla_\theta \ell(\theta_0^{(k)})\right\|^2 + 3\sigma^2\right).$$

Proof. By definition, $\theta_q^{(k)} - \theta_0^{(k)} = \frac{\alpha_k}{NB}\sum_{p=1}^q \sum_{i,j\in C_p} \nabla_\theta \ell_{i,j}(\theta_{p-1}^{(k)})$. Then, by using Cauchy-Schwarz's inequality $\|\sum_{i=1}^n a_i\|^2 \leq n\sum_{i=1}^n \|a_i\|^2$ repeatedly, we have

$$\begin{aligned}
&\|\theta_q^{(k)} - \theta_0^{(k)}\|^2\\
&\leq \frac{3\alpha_k^2 q^2 B^2}{N^2}\Bigg[\|\frac{1}{qB^2}\sum_{p=1}^q\sum_{i,j\in C_p}\left(\nabla_\theta \ell_{i,j}(\theta_{p-1}^{(k)}) - \nabla_\theta \ell_{i,j}(\theta_0^{(k)})\right)\|^2 +\\
&\qquad \|\frac{1}{qB^2}\sum_{p=1}^q\sum_{i,j\in C_p}\left(\nabla_\theta \ell_{i,j}(\theta_0^{(k)}) - \nabla_\theta \ell(\theta_0^{(k)})\right)\|^2 + \|\nabla_\theta \ell(\theta_0^{(k)})\|^2\Bigg]\\
&\leq \frac{3\alpha_k^2 q^2 B^2}{N^2}\Bigg[\frac{1}{qB^2}\sum_{p=1}^q\sum_{i,j\in C_p}\|\nabla_\theta \ell_{i,j}(\theta_{p-1}^{(k)}) - \nabla_\theta \ell_{i,j}(\theta_0^{(k)})\|^2 +\\
&\qquad \frac{1}{qB^2}\sum_{i,j=1}^N \|\nabla_\theta \ell_{i,j}(\theta_0^{(k)}) - \nabla_\theta \ell(\theta_0^{(k)})\|^2 + \|\nabla_\theta \ell(\theta_0^{(k)})\|^2\Bigg]\\
&\leq \frac{3\alpha_k^2 q^2 B^2}{N^2}\left[\frac{L^2}{q}\sum_{p=1}^q \|\theta_{p-1}^{(k)} - \theta_0^{(k)}\|^2 + \frac{N^2}{qB^2}\left(M\|\nabla_\theta \ell(\theta_0^{(k)})\|^2 + \sigma^2\right) + \|\nabla_\theta \ell(\theta_0^{(k)})\|^2\right]\\
&\leq \frac{3\alpha_k^2 L^2 B^2 q}{N^2}\Delta + 3\alpha_k^2\left[q\left(M\|\nabla_\theta \ell(\theta_0^{(k)})\|^2 + \sigma^2\right) + \frac{q^2B^2}{N^2}\|\nabla_\theta \ell(\theta_0^{(k)})\|^2\right],
\end{aligned}$$

where we have used the assumptions (A.2) and (A.3) in the second last inequality. Summing from 1 to $\frac{N}{B}$,

$$\Delta = \sum_{q=1}^{\frac{N}{B}} \|\theta_{q-1}^{(k)} - \theta_0^{(k)}\|^2 \leq \frac{3\alpha_k^2 L^2}{2}\Delta + \frac{3\alpha_k^2 N^2}{2B^2}\left(M\left\|\nabla_\theta \ell(\theta_0^{(k)})\right\|^2 + \sigma^2\right) + \frac{\alpha_k^2 N}{B}\left\|\nabla_\theta \ell(\theta_0^{(k)})\right\|^2.$$

Since $\alpha_k \leq \frac{1}{L\sqrt{3}}$, then $\frac{3\alpha_k^2 L^2}{2} \leq \frac{1}{2}$. Therefore,

$$\Delta \leq \frac{\alpha_k^2 N^2}{B^2}\left((3M+2)\left\|\nabla_\theta \ell(\theta_0^{(k)})\right\|^2 + 3\sigma^2\right).$$

□

Lemma B.2. *Suppose that assumption (A.2) holds. Let learning rate $\alpha_q^{(k)} := \alpha_k \frac{B}{N} > 0$ for a given sequence $\{\alpha_k\}$ such that $0 < \alpha_k \le \frac{1}{L}$. Then we have*

$$\ell(\theta_{k+1}) \le \ell(\theta_k) + \frac{\alpha_k L^2 B}{2N} \sum_{q=1}^{\frac{N}{B}} \|\theta_k - \theta_{q-1}^{(k+1)}\|^2 - \frac{\alpha_k}{2}\|\nabla \ell(\theta_k)\|^2 .$$

Proof. By assumption (A.2), ℓ is also L-smooth. Then we derive

$$\begin{aligned}
\ell(\theta_{k+1}) &\le \ell(\theta_k) + \langle \nabla \ell(\theta_k), \theta_{k+1} - \theta_k\rangle + \frac{L}{2}\left\|\theta_{k+1} - \theta_k\right\|^2 \\
&= \ell(\theta_k) - \frac{\alpha_k}{NB}\langle \nabla \ell(\theta_k), \sum_{q=1}^{\frac{N}{B}} \sum_{i,j\in C_q} \nabla_\theta \ell_{i,j}(\theta_{q-1}^{(k+1)})\rangle + \frac{L}{2}\frac{\alpha_k^2}{N^2B^2}\|\sum_{q=1}^{\frac{N}{B}} \sum_{i,j\in C_q} \nabla_\theta \ell_{i,j}(\theta_{q-1}^{(k+1)})\|^2 \\
&= \ell(\theta_k) + \frac{\alpha_k}{2}\|\nabla \ell(\theta_k) - \frac{1}{BN}\sum_{q=1}^{\frac{N}{B}} \sum_{i,j\in C_q} \nabla_\theta \ell_{i,j}(\theta_{q-1}^{(k+1)})\|^2 - \frac{\alpha_k}{2}\|\nabla \ell(\theta_k)\|^2 \\
&\quad + \left(\frac{L}{2}\frac{\alpha_k^2}{N^2B^2} - \frac{\alpha_k}{2N^2B^2}\right)\|\sum_{q=1}^{\frac{N}{B}} \sum_{i,j\in C_q} \nabla_\theta \ell_{i,j}(\theta_{q-1}^{(k+1)})\|^2 ,
\end{aligned}$$

where last equality uses the identity $ab = \frac{1}{2}(a^2 + b^2 - (a-b)^2)$. Since $\alpha_k \le \frac{1}{L}$, then we have $\frac{L}{2}\frac{\alpha_k^2}{N^2B^2} - \frac{\alpha_k}{2N^2B^2} \le 0$. Thus,

$$\begin{aligned}
\ell(\theta_{k+1}) &\le \ell(\theta_k) + \frac{\alpha_k}{2}\|\nabla \ell(\theta_k) - \frac{1}{BN}\sum_{q=1}^{\frac{N}{B}} \sum_{i,j\in C_q} \nabla_\theta \ell_{i,j}(\theta_{q-1}^{(k+1)})\|^2 - \frac{\alpha_k}{2}\|\nabla \ell(\theta_k)\|^2 \\
&\le \ell(\theta_k) + \frac{\alpha_k}{2}\frac{1}{BN}\sum_{q=1}^{\frac{N}{B}} \sum_{i,j\in C_q} \|\nabla \ell(\theta_k) - \nabla_\theta \ell_{i,j}(\theta_{q-1}^{(k+1)})\|^2 - \frac{\alpha_k}{2}\|\nabla \ell(\theta_k)\|^2 \\
&\le \ell(\theta_k) + \frac{\alpha_k L^2 B}{2N}\sum_{q=1}^{\frac{N}{B}} \|\theta_k - \theta_{q-1}^{(k+1)}\|^2 - \frac{\alpha_k}{2}\|\nabla \ell(\theta_k)\|^2 .
\end{aligned}$$

□

Acknowledgments

LW would like to thank Prof. Jose A. Carrillo and Dr. Jeremy Wu for inspiring discussion on gradient flow formulation of the Landau equation. We also acknowledge ChatGPT for its assistance in refining the language and improving the clarity of the manuscript.

References

[1] L. Ambrosio, N. Gigli, and G. Savaré, *Gradient Flows: In Metric Spaces and in the Space of Probability Measures*, Birkhäuser Basel, 2005.

[2] R. Bailo, J. A. Carrillo, and J. Hu, *The collisional particle-in-cell method for the Vlasov-Maxwell-Landau equations*, arXiv preprint arXiv:2401.01689, (2024).

[3] J.-D. Benamou and Y. Brenier, *A computational fluid mechanics solution to the Monge-Kantorovich mass transfer problem*, Numerische Mathematik, 84 (2000), pp. 375–393.

[4] L. Bottou, F. E. Curtis, and J. Nocedal, *Optimization methods for large-scale machine learning*, SIAM Review, 60 (2018), pp. 223–311.

[5] C. Buet and S. Cordier, *Conservative and entropy decaying numerical scheme for the isotropic Fokker–Planck–Landau equation*, Journal of Computational Physics, 145 (1998), pp. 228–245.

[6] J. A. Carrillo, K. Craig, L. Wang, and C. Wei, *Primal dual methods for Wasserstein gradient flows*, Foundations of Computational Mathematics, 22 (2022), pp. 389–443.

[7] J. A. Carrillo, M. G. Delgadino, L. Desvillettes, and J. S. H. Wu, *The Landau equation as a gradient flow*, Analysis and PDE, 17 (2024), pp. 1331–1375.

[8] J. A. Carrillo, J. Hu, L. Wang, and J. Wu, *A particle method for the homogeneous Landau equation*, Journal of Computational Physics: X, 7 (2020), p. 100066.

[9] J. A. Carrillo, S. Jin, and Y. Tang, *Random batch particle methods for the homogeneous Landau equation*, Communications in Computational Physics, 31 (2022), pp. 997–1019.

[10] J. A. Carrillo, D. Matthes, and M.-T. Wolfram, *Lagrangian schemes for Wasserstein gradient flows*, in Handbook of Numerical Analysis, vol. 22, Elsevier, 2021, pp. 271–311.

[11] J. A. Carrillo, L. Wang, and C. Wei, *Structure preserving primal dual methods for gradient flows with nonlinear mobility transport distances*, SIAM Journal on Numerical Analysis, 62 (2024), pp. 376–399.

[12] G. Chen, L. Chacón, and D. C. Barnes, *An energy-and charge-conserving, implicit, electrostatic particle-in-cell algorithm*, Journal of Computational Physics, 230 (2011), pp. 7018–7036.

[13] R. T. Q. Chen, Y. Rubanova, J. Bettencourt, and D. K. Duvenaud, *Neural ordinary differential equations*, Advances in Neural Information Processing Systems, 31 (2018).

[14] P. Degond and B. Lucquin-Desreux, *The Fokker-Planck asymptotics of the Boltzmann collision operator in the Coulomb case*, Mathematical Models and Methods in Applied Sciences, 2 (1992), pp. 167–182.

[15] ———, *An entropy scheme for the Fokker-Planck collision operator of plasma kinetic theory*, Numerische Mathematik, 68 (1994), pp. 239–262.

[16] L. Desvillettes and C. Villani, *On the spatially homogeneous Landau equation for hard potentials part i : existence, uniqueness and smoothness*, Communications in Partial Differential Equations, 25 (2000), pp. 179–259.

[17] ———, *On the spatially homogeneous Landau equation for hard potentials part ii : h-theorem and applications*, Communications in Partial Differential Equations, 25 (2000), pp. 261–298.

[18] G. Dimarco, R. Caflisch, and L. Pareschi, *Direct simulation Monte Carlo schemes for Coulomb interactions in plasmas*, arXiv preprint arXiv:1010.0108, (2010).

[19] F. Filbet and E. Sonnendrücker, *Numerical methods for the Vlasov equation*, in Numerical Mathematics and Advanced Applications: Proceedings of ENUMATH 2001 the 4th European Conference on Numerical Mathematics and Advanced Applications Ischia, July 2001, Springer, 2003, pp. 459–468.

[20] W. Grathwohl, R. T. Q. Chen, J. Bettencourt, and D. Duvenaud, *Scalable reversible generative models with free-form continuous dynamics*, International Conference on Learning Representations, (2019).

[21] N. Guillen and L. Silvestre, *The Landau equation does not blow up*, arXiv preprint arXiv:2311.09420, (2023).

[22] Y. Guo, *The Landau equation in a periodic box*, Communications in Mathematical Physics, 231 (2002), pp. 391–434.

[23] K. He, X. Zhang, S. Ren, and J. Sun, *Deep residual learning for image recognition*, 2016 IEEE Conference on Computer Vision and Pattern Recognition (CVPR), (2016), pp. 770–778.

[24] Y. Huang and L. Wang, *A score-based particle method for homogeneous Landau equation*, arXiv preprint arXiv:2405.05187, (2024).

[25] V. Ilin, J. Hu, and Z. Wang, *Transport based particle methods for the Fokker-Planck-Landau equation*, arXiv preprint arXiv:2405.10392, (2024).

[26] S. Jin, L. Li, and J.-G. Liu, *Random batch methods (RBM) for interacting particle systems*, Journal of Computational Physics, 400 (2020), p. 108877.

[27] R. Jordan, D. Kinderlehrer, and F. Otto, *The variational formulation of the Fokker–Planck equation*, SIAM Journal on Mathematical Analysis, 29 (1998), pp. 1–17.

[28] L. D. Landau, *The kinetic equation in the case of Coulomb interaction*, tech. rep., General Dynamics/Astronautics San Diego Calif, 1958.

[29] W. Lee, L. Wang, and W. Li, *Deep JKO: time-implicit particle methods for general nonlinear gradient flows*, Journal of Computational Physics, (2024), p. 113187.

[30] W. Li, J. Lu, and L. Wang, *Fisher information regularization schemes for Wasserstein gradient flows*, Journal of Computational Physics, 416 (2020), p. 109449.

[31] L. M. Nguyen, Q. Tran-Dinh, D. T. Phan, P. H. Nguyen, and M. van Dijk, *A unified convergence analysis for shuffling-type gradient methods*, Journal of Machine Learning Research, 22 (2021), pp. 1–44.

[32] L. Pareschi, G. Russo, and G. Toscani, *Fast spectral methods for the Fokker–Planck–Landau collision operator*, Journal of Computational Physics, 165 (2000), pp. 216–236.

[33] C. Villani, *On a new class of weak solutions to the spatially homogeneous Boltzmann and Landau equations*, Archive for Rational Mechanics and Analysis, 143 (1998), pp. 273–307.

[34] ——, *On the spatially homogeneous Landau equation for Maxwellian molecules*, Mathematical Models and Methods in Applied Sciences, 08 (1998), pp. 957–983.

[35] ——, *Topics in Optimal Transportation*, Graduate Studies in Mathematics, American Mathematical Society, 2003.